PREDIS

Deliverable 7.3

Innovative Integrity Testing and Monitoring Techniques

2024-02-19 Version 1.2 Final

Dissemination level: Public

Christan Köpp & Ernst Niederleithinger
Bundesanstalt für Materialforschung und -prüfung (BAM)
Unter den Eichen 87, 12205 Berlin, Germany

email: christian.koepp@bam.de, ernst.niederleithinger@bam.de

This project has received funding from the Euratom research and training programme 2019-2020 under grant agreement No 945098.

Project acronym PREDIS	Project title PRE-DISposal management of radioactive waste		Grant agreement No. 945098
Deliverable No. D7.3	Deliverable title Innovative Integrity Testing and Monitoring Techniques		Version 1.2
Type Report	Dissemination level Public		Due date M42
Lead beneficiary BAM			WP No. 7.3
Main author Christian Köpp and Ernst Niederleithinger (BAM)	Reviewed by Ernst Niederleithinger (BAM), WP7 Lead	Accepted by Maria Oksa (VTT), Coordinator	
Contributing authors M. Romoli - INFN Naples Unit, P. Finocchiaro - INFN LNS Unit, P. Andreetto, P. Checchia, E. Conti, F.Gonella - INFN Padua Unit C. Sabbarese, A. D'Onofrio - UNICAMPANIA (LTP) Andrea Chierici, Rosa Lo Frano, Riccardo Ciolini, Francesco d'Errico, Department of Industrial and Civil Engineering - UNIPI Gert Dekkers, Dylan Gybels - Magics Technologies Omer Elnasaney, Darren Potter - National Nuclear Laboratory Leone Pasquato, Christoph Strangfeld, Ernst Niederleithinger, Christian Köpp - BAM Esko Strömmer, Marko Korkalainen - VTT			Pages 74

Abstract

This work is a part of the European project, PREDIS, on pre-disposal treatment and management of low-level waste and intermediate-level waste, The state of the art report (D7.1) and the gap analysis (WP2) have identified the need for more research on adequate and industrially mature solutions (practices, data governance, technology, and tools) for monitoring the packages and supporting decisions in the preparation, handling, and long-term interim storage of low-level/intermediate-level cemented waste.

Within the work package 7 "Innovations in cemented waste handling and pre-disposal storage", the main objective of task T7.3 is to optimise innovative integrity testing and monitoring techniques. Three sub-tasks are specifically dealing with

T7.3.1 External sensing technologies,

T7.3.2 Embedded sensing technologies in an instrumented package and

T7.3.3 Preliminary system testing and optimisation.

In this deliverable, the results of T 7,3 are compiled into a report on "Innovative Integrity Testing and Monitoring Techniques".Overall, the specific reports show the progress already made during the project time so far. The prototypes are ready for use under realistic conditions and partly have already successfully been tested in virtual and laboratory environments.

D7.3 can be considered as an update to the milestone report MS53 which is now obsolete.

D7.3 describes the techniques, methods and devices delevoped, their functionality and test results. An evaluation and recommendations will be part of the work done in T 7.6 and the values assessement performed by WP2

Coordinator Contact

Maria Oksa

VTT Technical Research Centre of Finland Ltd

Kivimiehentie 3, Espoo / P.O. Box 1000, 02044 VTT, Finland

E-mail: maria.oksa.@vtt.fi, Tel: +358 50 5365 844

Acknowledgment

This project has received funding from the Euratom research and training programme 2019-2020 under grant agreement No 945098.

HISTORY OF CHANGES

Date	Version	Author	Comments
10.2.2024	1.0	BAM; VTT, INFN, UNIPI, MAGICS, NNL	Draft version for internal review
15.2.2024	1.1	BAM; VTT, INFN, UNIPI, MAGICS, NNL	Final version for internal review
19.02.2024	1.2	BAM	Review by WP lead

CONTENT

1 Introduction

Ernst Niederleithinger, Christian Köpp
Bundesanstalt für Materialforschung und -prüfung, Berlin, Germany

Within the work package 7 “Innovations in cemented waste handling and pre-disposal storage”, the task T7.3 is optimising innovative integrity testing and monitoring techniques. Three sub-tasks are specifically dealing with

- T7.3.1 External sensing technologies,
- T7.3.2 Embedded sensing technologies in an instrumented package and
- T7.3.3 Preliminary system testing and optimisation.

In this deliverable, the work relevant for the milestone MS53 “Prototypes ready for demonstrations in real environments” is described by individual partners to summarise the following aspects:

- A description of the method/technique used
- work accomplished already within the PREDIS project showing the test scenarios
- outcomes, upcoming developments and future tests/directions.

Overall, the specific reports show the progress already made during the project time so far. The prototypes are ready for use under realistic conditions and partly have already successfully been tested in virtual and laboratory environments.

D7.3 can be considered as an update tp milestone report MS53 which is now obsolete.

D7.3 describes the techniques, methods and devices delevoped, their functionality and test results. An evaluation and recommendations will be part of the work done in T 7.6 and the values assessement performed by WP2

2 Sensing technology: SciFi (gamma) and SiLiF (neutron) radiation monitoring

M. Romoli - INFN Naples Unit
P. Finocchiaro - INFN LNS Unit
P. Checchia, E. Conti - INFN Padua Unit
C. Sabbarese, A. D'Onofrio - UNICAMPANIA (LTP)

2.1 Background

The PREDIS (Predisposal management of radioactive waste) Euratom project is aimed at the development and implementation of activities for predisposal treatment of radioactive waste streams other than nuclear fuel and high-level radioactive waste [0/1]. Within the Work Package 7 the project contemplates to test and evaluate innovative tools and techniques in cemented waste handling and predisposal storage, and in particular to demonstrate the feasibility of medium-to-long term monitoring by means of low-cost radiation sensors to be installed around the radwaste drums. A periodic automatic check of the radiation levels around radwaste drums could represent an added value with respect to safety and security, with recorded streams of count-rate data providing a useful tool for an early detection of possible anomalies or tampering with the drums. The enhancement in terms of transparency is noteworthy as well [0/2-2/5].

2.2 Method

SciFi [0/6] and SiLiF [0/7] radiation sensors have been developed by INFN in the past years and have been successfully tested to be used as gamma and neutron detectors with readout chains based on standard nuclear electronics modules [0/8]. In the framework of PREDIS we considered the possibility of employing such detectors developing a custom electronics board with some particular features: high modularity and re-configurability (to ensure fast and easy maintenance), battery operation, WiFi connection for data transfer and remote control, low power consumption, temperature measured on board.

The proposed monitoring method relies on a number of SciFi and SiLiF sensors, say four of each kind, to be hung to the cemented drum for monitoring purpose during the whole predisposal phase. Before and after its full characterization each drum would be monitored for possible anomalies arising in the meantime while waiting for disposal.

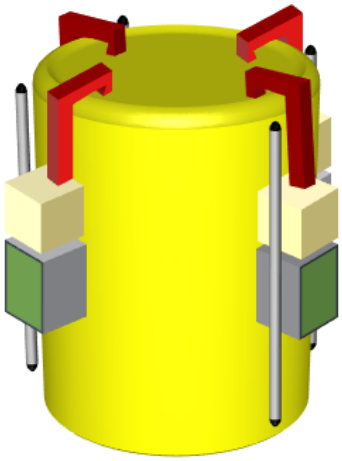

Fig. 1. A possible arrangement of four radiation monitoring units on a cemented drum during its predisposal phase.

2.3 Technical Development

Each detection unit consists of

- a SciFi gamma ray detector [0/6] coupled to its front-end electronics, data acquisition and transmission, which are allocated inside a dedicated box;
- a SiLiF neutron detector [0/7], coupled to its front-end electronics, data acquisition and transmission, which are allocated inside a dedicated box.

The SciFi features a 3 mm diameter, 80 cm long, scintillating optical fiber [0/9] coupled at each end to a MicroFC-30035-SMT SiPM produced by ON Semiconductor [0/10]. A SciFi unit is shown in Fig.2, with the logical operating principle sketched in Fig.3. A SiLiF unit consists of a double-sided 3×3 cm^2 silicon detector sandwiched between two layers of ^{6}LiF neutron converter deposited on carbon fiber substrates. The sandwich is enclosed in a suitable 10×10×10 cm^3 polyethylene moderator. On occurrence of a neutron capture in ^{6}Li two high energy particles are produced, an alpha and a triton, which are then likely to be detected by the silicon diode. Fig. 4 illustrates the components of a SiLiF sensor.

Fig.2. The SciFi detector consisting of a 3 mm diameter, 80 cm long, scintillating fiber coupled at each end to a SiPM and enclosed in an aluminium pipe.

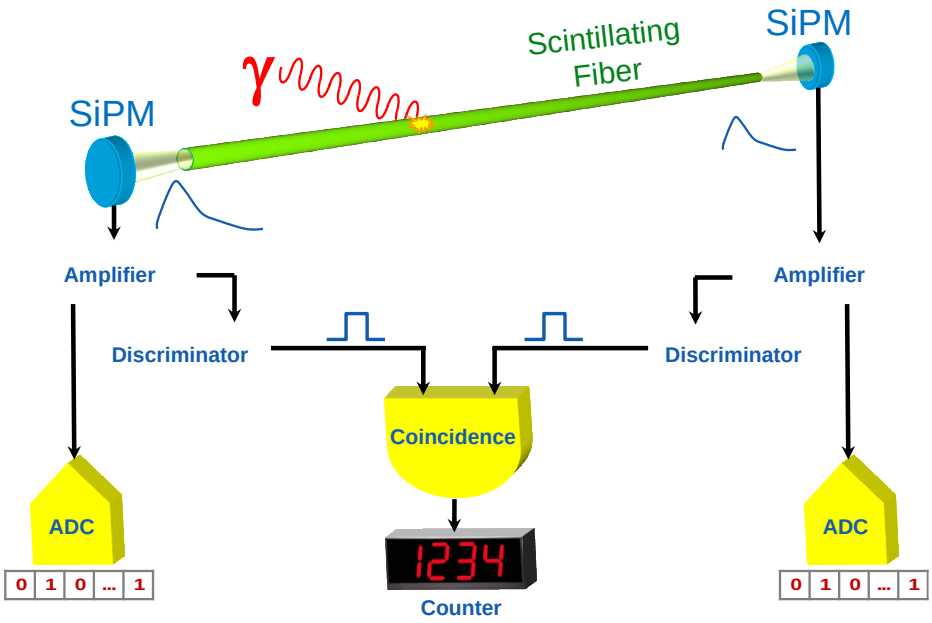

Fig.3. Sketch of the logical operating principle of a SciFi gamma ray detector.

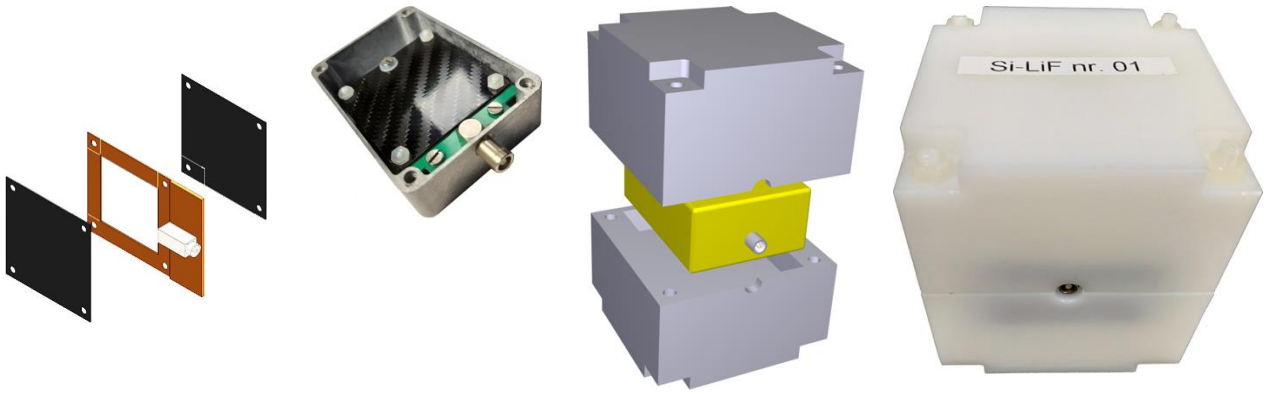

(a) (b) (c) (d)

Fig. 4. (a) sketch of the silicon sandwiched between two ^{6}LiF layers deposited on carbon fiber. (b) The sandwich assembled inside its aluminium box. (c) 3D sketch of the detector assembly inside its PET moderator. (d) A SiLiF sensor fully assembled.

The newly developed readout and data acquisition electronics, shown in Fig.5, can handle either a SciFi or a SiLiF sensor, providing the required bias voltage and featuring preamplifiers, analog to digital conversion, local data storage, WiFi control and data transfer, by means of a dedicated onboard ESP32 microcontroller. Moreover, the output bias voltage and the board temperature can be measured, while a low consumption Bluetooth receiver is used to wake-up the system when in sleep mode. Each board, powered by batteries or via USB connection, can be programmed to perform periodic cycles of wake-up, measurement, and sleep. A complete radiological monitoring unit, consisting of one SciFi and one SiLiF with their respective electronics boxes, is shown in Fig.6.

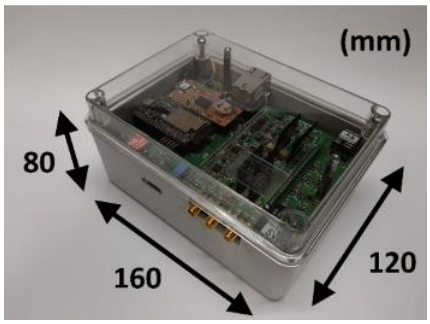

Fig.5. New electronics with package size.

Fig.6. A complete monitoring unit consisting of one SiLiF and one SciFi detectors with the related electronics.

2.4 Lab tests

The typical amplitude spectra of the signals from the SiPMs at the two ends of a SciFi sensor detecting gamma rays are shown in Fig.7. The scintillation light produced by the fiber, when exposed to a gamma ray source, gives rise to the multi-peak structure reflecting the discrete numbers of detected photons [2/11-2/14]. Shown is the threshold set on the discriminators (Fig.3) at four photons, required to suppress the spurious noise along with the required coincidence between the signals at the two detector ends [2/7]. The large peak around channel 350, due to the saturation of the amplifier, does not pose any detection problem. The histogram in Fig.8 shows the distribution of the B/A event-by-event ratio between the signal amplitudes measured at the two ends of a SciFi sensor exposed to a ^{137}Cs gamma source. As expected, the histogram is narrow and centered at 1. Many measurements have been performed in laboratory with calibration sources to study the stability of the newly developed electronics, producing quite satisfactory results.

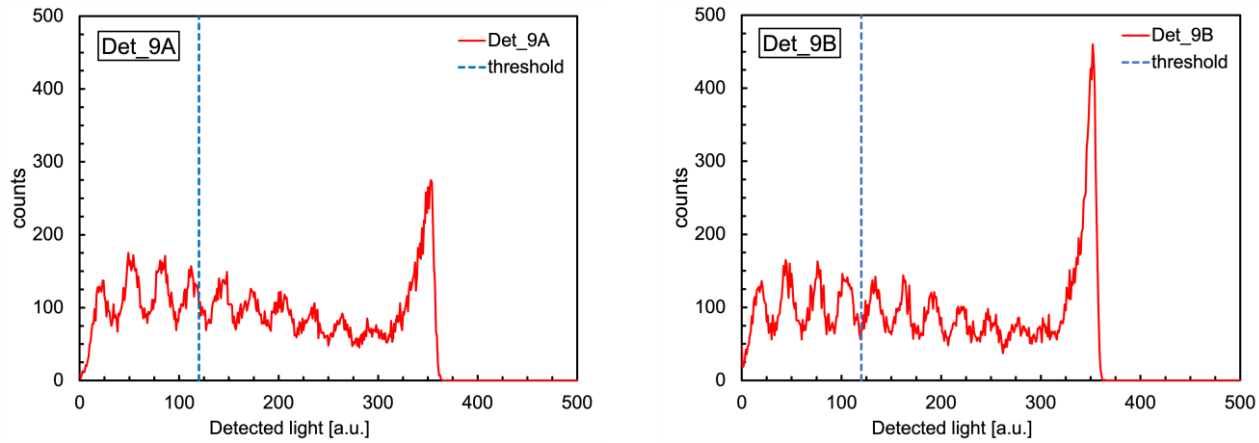

Fig.7. Typical amplitude spectra of the signals from the SiPMs at the two ends of a SciFi sensor. The scintillation light produced by the fiber when exposed to a gamma ray source gives rise to the multi-peak structure reflecting the discrete numbers of detected photons. Shown is the threshold at four photons required to suppress the spurious noise. The large peak around channel 350 is due to the saturation of the amplifier.

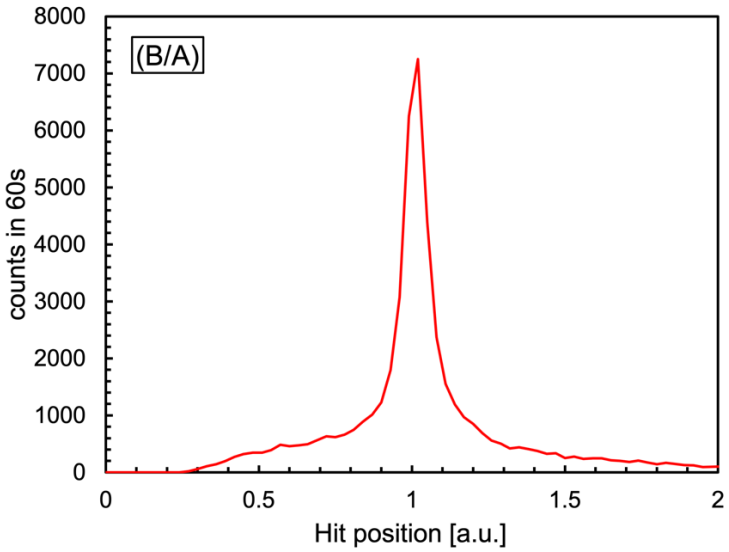

Fig.8. Distribution of the B/A ratio of the signal amplitudes detected by the two SiPMs of a SciFi sensor exposed to a ^{137}Cs gamma source.

The SiLiF detectors have been extensively tested with neutron sources, and their solid blindness to gamma rays has been assessed [2/7]. In Fig. 9 the deposited energy spectrum measured by a SiLiF detector exposed to a PuBe source is shown, in linear (a) and logarithmic (b) scale. The plot exhibits the expected typical whale shape, whereas the background (in the UJV Řež underground storage site), measured without the source, is rather low but non-negligible with a signal to background ratio about 10^{-4}. The neutron discrimination threshold is chosen at 1.5 MeV to exploit a gamma/neutron rejection below 10^{-8}.

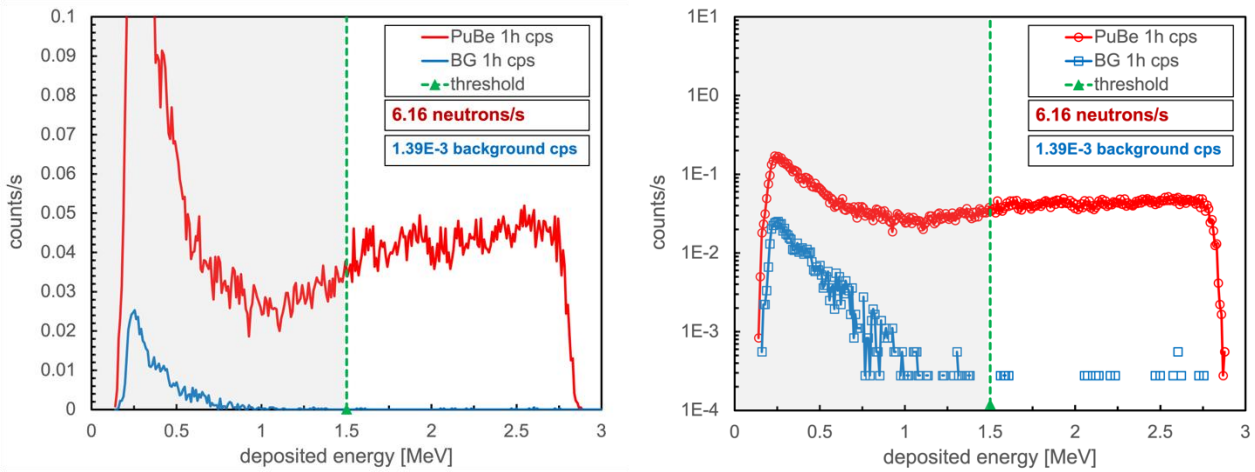

Fig. 9. Deposited energy spectrum measured by a SiLiF detector exposed to a PuBe source, in linear (a) and logarithmic (b) scale.

2.5 Test in a realistic environment

The demonstration test of this technology was performed in a realistic environment, an underground radwaste storage room on the premises of UJV at Řež (Prague). A 200 l concrete mockup, 820 mm high with 571 mm diameter and encased into a 1.2 mm thick galvanized steel drum, was built on purpose for the test. Its structure, shown in Fig. 10, was initially meant to allow for the insertion of one or more radioactive sources in vertical holes running through its full height, giving rise externally to a non-uniform radiation field to be detected and measured. The non-uniformity was foreseen to characterize the behaviour of the sensors in response to such a field, showing that they would be capable of detecting asymmetries and/or deviations from the average, should anomalies occur to a real drum so equipped. Due to logistic and radiation protection reasons a single configuration was chosen for the final demo, with a 165 MBq ^{137}Cs gamma source placed into the quasi-central hole, and the drum was equipped with four sensor units to monitor it during a two-month period.

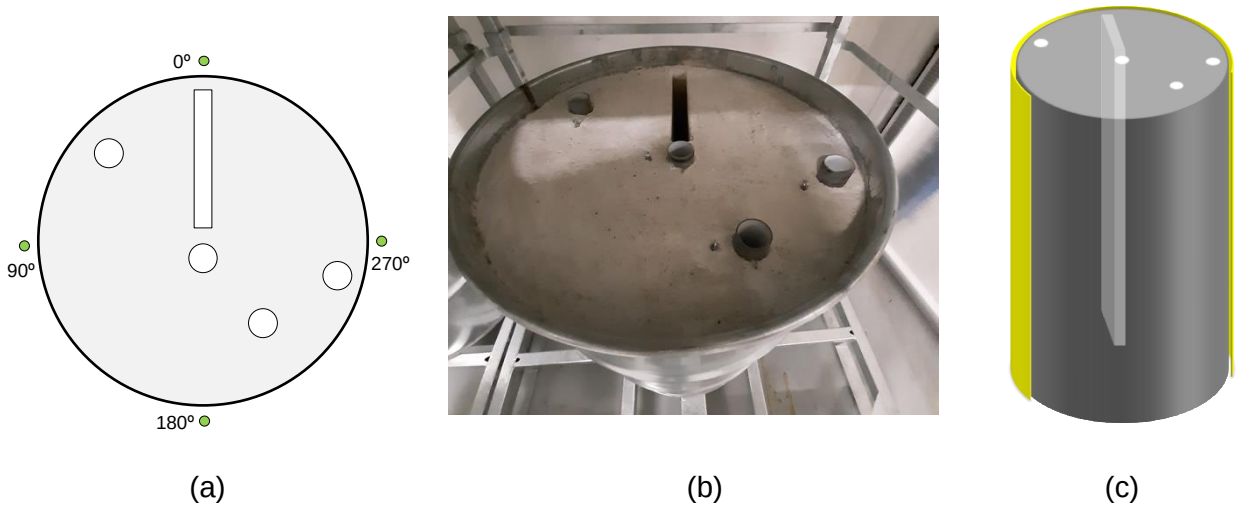

*Fig. 10. (**a**) Top view of the mockup scheme; the four green circles (0°, 90°, 180°, 270°) indicate the position of the SciFi sensors; the white rectangle and circles represent the vertical holes in the concrete cylinder. (**b**) A top picture of the cemented mockup drum, with the lid removed. (**c**) A 3D sketch of the mockup inside; part of the steel skin is highlighted in yellow, the concrete is in grey, the vertical holes in light grey.*

Simulations have been performed highlighting the possibility to use such detectors to hint at anomalies (crack?) of the concrete inside a drum by detecting changes in the emitted radiation counting rates. The mockup geometry of Fig. 10 was reproduced in FLUKA [0], including the four SciFi detectors around the drum. 10^9 decays from the above mentioned ^{137}Cs gamma source were simulated and tracked, finally producing: (i) a 3D map of the expected dose rate distribution; (ii) the deposited energy spectra on the four SciFi fibers. Fig. 11a shows the expected dose distribution on an XY cross section at mid-height of the drum (40 cm < Z < 41 cm). Fig. 11b represents the XY dose rate averaged along the full height of the drum. Fig. 12a depicts the expected dose distribution on a YZ cross section with -1 cm < X < 1 cm. Finally, in Fig. 12b the expected dose rate distribution on the drum surface is represented in 3D, with three scintillating fibers also visible. Table 1 lists the simulated dose rate at three different heights in the 0° and 180° position around the drum. Shown for comparison are also the dose rates measured with a handheld instrument. The differences, not so large indeed, seemed to be ascribed on the one hand to the uncertainty in the source position and in the positioning of the instrument on the other hand. Unsurprisingly, the agreement looks quite reasonable.

Table 1. Simulated and measured dose rates at three different heights in the 0° and 180° position around the drum. See the text for an explanation of the differences.

position	dose rate at 0° [µSv/h]		dose rate at 180° [µSv/h]	
	simulated	measured	simulated	measured
high	35	45	2	1.5
middle	115	80	22	15
low	35	25	2	3

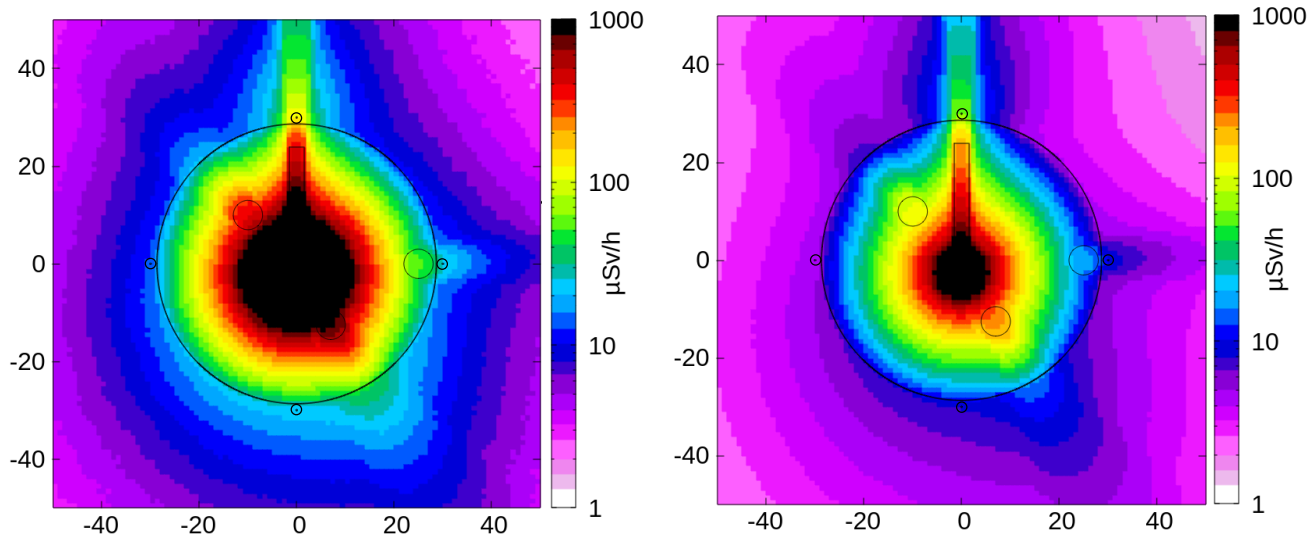

Fig. 11. FLUKA simulation of the 165 MBq ^{137}Cs gamma source placed at mid-height inside the quasi-central hole of the mockup. All dimensions are in cm. (a) Expected dose distribution on an XY cross section at mid-height of the drum (40 cm < Z < 41 cm). (b) Expected XY dose rate averaged along the full height of the drum.

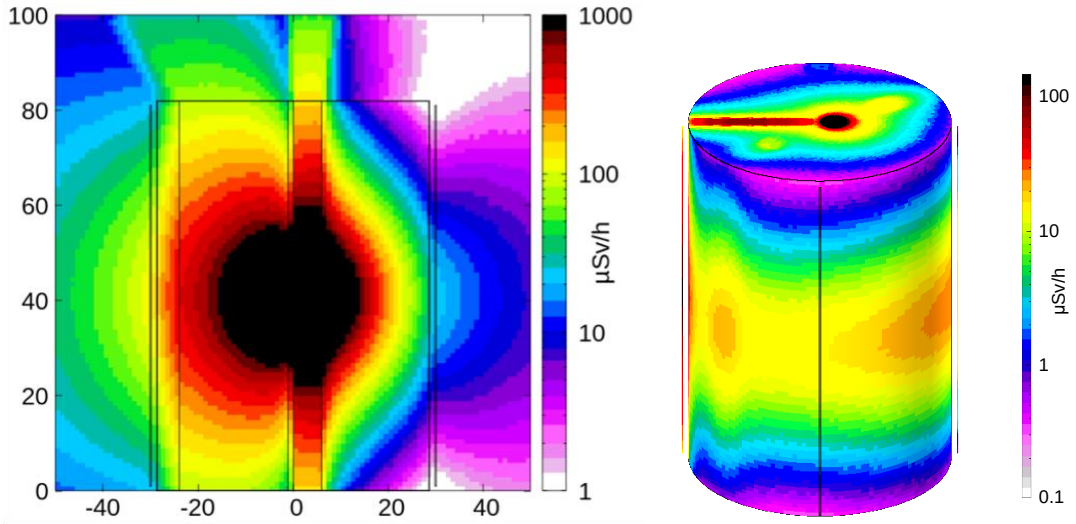

(a) (b)

Fig. 12. FLUKA simulation of the 165 MBq ^{137}Cs gamma source placed at mid-height inside the quasi-central hole of the mockup. (a) Expected dose distribution on a YZ cross section with −1 cm < X < 1 cm. (b) 3D representation of the expected dose rate distribution on the drum surface, three scintillating fibers are also visible.

As already mentioned, due to logistic reasons mainly related to the high source activity and the consequent radiation protection issues, along with the limited access to the storage site and to the mockup drum, it was decided to run a single demonstration with the radioactive source inserted in the quasi-central hole. The four sensor units were hung to the drum and initially connected via wires for their preliminary set-up and tuning, as shown in Fig. 13a. Several drums filled with concrete were placed beside and over the mockup (Fig. 13b), then the wires were disconnected and other drums with concrete were placed in front (Fig. 14), in order to also verify the signal transmission capability through such a heavy shielding. The sensors, interfaced to a local server through a WiFi connection, were programmed to wake up every six hours and acquire data for one minute. The local server was connected to a network router with a public IP address and thus reachable remotely via a Virtual Private Network (VPN). Indeed, this configuration enabled the authorized users to interact remotely with the server, to download the measured data, and if needed with each sensor for possible set-up changes. An additional sensor was installed about six meters away in the same room to measure the ambient background. Since there was only a gamma source installed, no meaningful neutron counting rate was detected.

The raw counting rate data for the five SciFi sensors collected between 17-Nov-2023 and 15-Jan-2024 are plotted in Fig. 15. The normal sensor behaviour was assumed to be when the counting rate fluctuations kept within ±5 standard deviations, to account for any possible electrical or mechanical disturbance. However, one can see immediately that this was not enough: in a few cases some spikes showed up, but since these were spot events one can assume they were due to some unspecified noise. One can also observe that there are also increasing and decreasing trends in the counting rates of all sensors during corresponding time intervals. By looking at Fig. 16, which shows the temperature on the electronic boards, an anticorrelation is evident between counting rate change and temperature change. By using the data collected until 10-Dec-2023 such a correlation was quantified with linear coefficients and was used to correct the raw counting rate data for the temperature effect. Indeed, such an effect is due to the temperature behaviour of the electronics, as the SiPM gain drift with temperature is much less pronounced as can be seen on its datasheet [18]. The full data set, corrected for temperature changes, is shown in Fig. 17. A residual oscillating trend can be observed, as the temperature correction is not perfect, however the corrected data stay well within the ±5 standard deviations.

(a) (b)

Fig. 13. (a) The four SciFi sensors hung to the drum (along with other sensors not discussed here) initially connected via wires for preliminary setting up and tuning. (b) Several drums filled with concrete were placed beside and over the mockup.

Fig. 14. The final demo configuration, the wires were disconnected and other drums filled with concrete were placed in front of the mockup.

At the end of the demonstration another simple test was done, to check whether the sensors were well centered with respect to the assumed angular positions. The SciFi sensor number 9, nominally placed at 0° with respect to the rectangular missing wedge, was displaced to a few positions in steps of 4°. The corresponding counting rates were plotted versus the nominal position (Fig. 18) and we discovered that indeed the sensor was displaced by about 4° with respect to the real zero. The result of this test, that also explains the discrepancy reported in Table 1, is a further proof that the SciFi detector provides a sensitive tool to monitor the full drum height at once.

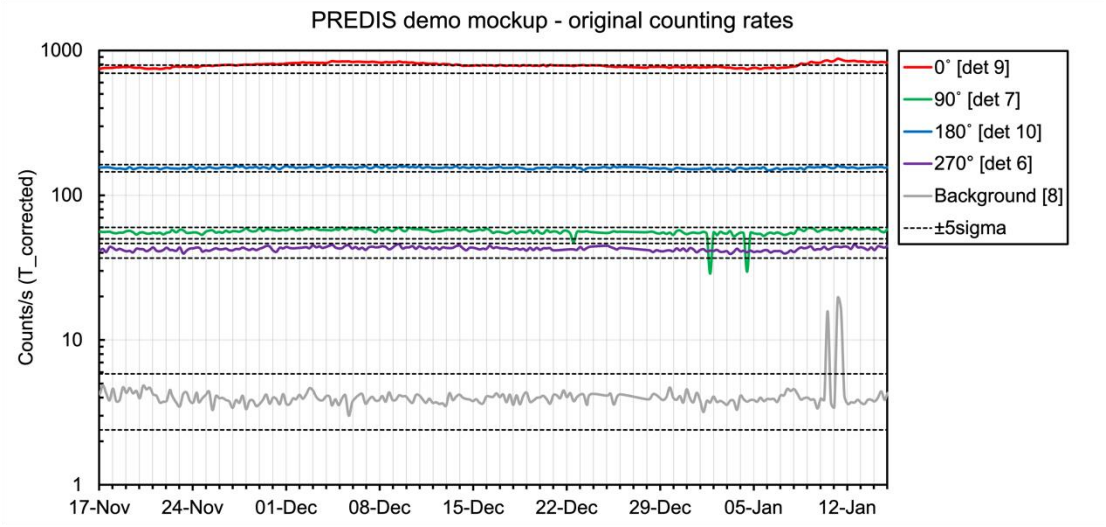

Fig. 15. Raw counting rate data collected between 17-Nov-2023 and 15-Jan-2024.

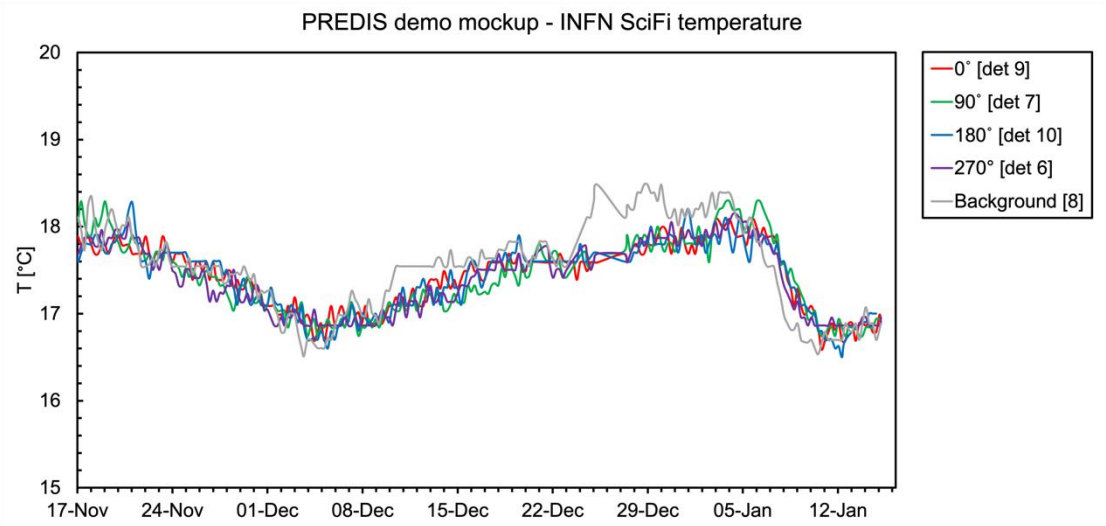

Fig. 16. Temperature measured on the five electronic boards throughout the test.

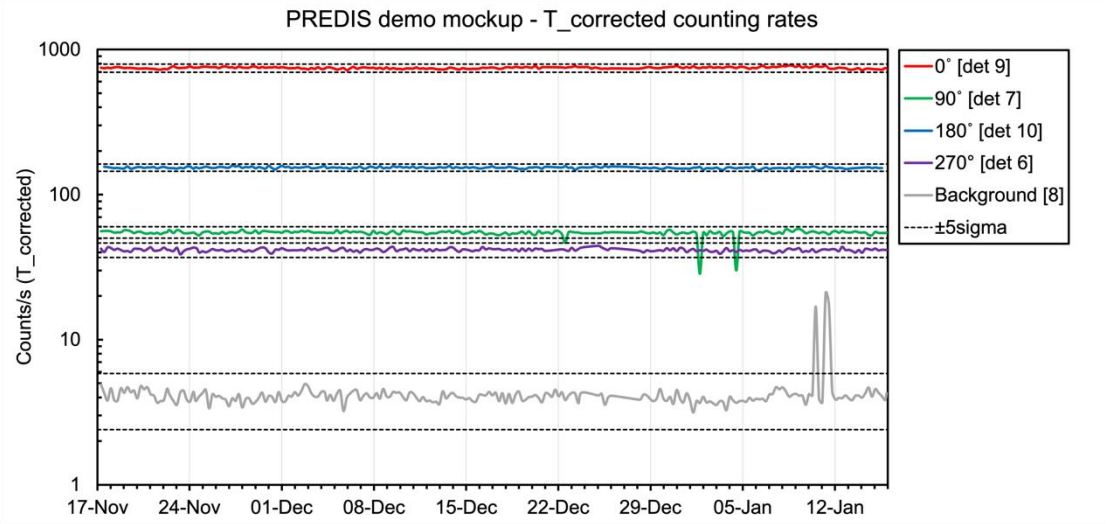

Fig. 17. The counting rate data collected between 17-Nov-2023 and 15-Jan-2024 corrected for the temperature changes.

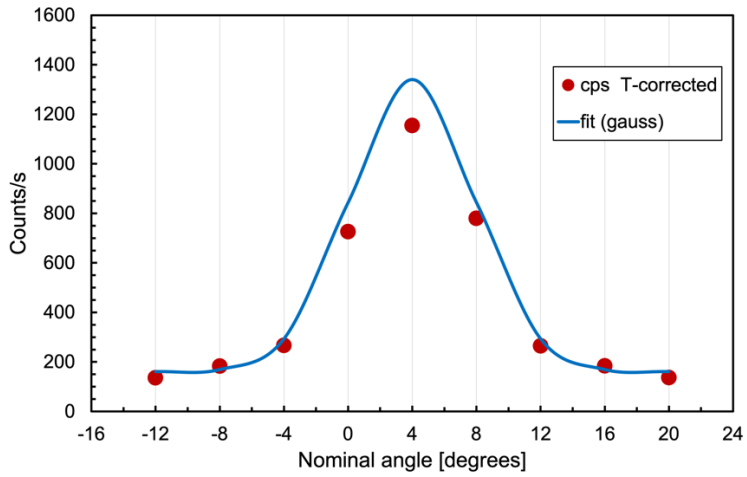

Fig. 18. Result of a drum scan around the nominal zero position using the SciFi number 9. It was discovered that the real zero was displaced by about 4°.

2.6 Summary and Outlook

The feasibility of medium-to-long term monitoring by means of radiation sensors to be installed around the radwaste drums was assessed by preliminary laboratory tests, simulations, and a 2-month data collection in a demonstration with a cemented mockup drum and a 165 MBq ^{137}Cs gamma source. The feasibility of neutron measurement was assessed separately by means of a PuBe neutron source. A periodic automatic check of the radiation levels around radwaste drums, as an added value with respect to safety and security, can be attained by recording streams of count-rate data from the sensors proposed within PREDIS. Such a monitoring technique, we believe, could represent soon a useful tool for an early detection of possible anomalies or tampering with the drums during their predisposal phase.

2.7 References

2/1 PREDIS project, Euratom H2020, GA No. 945098. Available online: https://predis-h2020.eu/ (accessed on 30 Nov 2023).

2/2 Finocchiaro, P. DMNR: A new concept for real-time online monitoring of short and medium term radioactive waste. In Radioactive Waste: Sources, Types and Management; Nova Science Publishers: New York, NY, USA, 2011; pp. 1-40.

2/3 Finocchiaro, P. Radioactive Waste: A System for Online Monitoring and Data Availability. Nucl. Phys. News 2014, 24, 34.

2/4 Cosentino, L.; Calì, C.; De Luca, G.; Guardo, G.; Litrico, P.; Pappalardo, A.; Piscopo, M.; Scirè; C.; Scirè; S.; Vecchio, G.; et al. Real-Time Online Monitoring of Radwaste Storage: A Proof-of-Principle Test Prototype. IEEE Trans. Nucl. Sci. 2012, 59, 1426–1431.

2/5 Finocchiaro, P.; Ripani, M.; Radioactive Waste Monitoring: Opportunities from New Technologies. In Proceedings of the IAEA International Conference on Physical Protection of Nuclear Material and Nuclear Facilities, IAEA-CN-254/117, Vienna, Austria, 13–17 November 2017.

2/6 Cosentino,L.; Giuffrida, M.; Lo Meo, S.; Longhitano, F.; Pappalardo, A.; Passaro, G.; Finocchiaro, P. Gamma—Ray Counters to Monitor Radioactive Waste Packages in the MICADO Project. Instruments 2021, 5, 19. https://doi.org/10.3390/

2/7 Cosentino, L.; Ducasse, Q.; Giuffrida, M.; Lo Meo, S.; Longhitano, F.; Marchetta, C.; Massara, A.; Pappalardo, P.; Passaro, G.; Russo, S.; Finocchiaro, P. SiLiF Neutron Counters to Monitor Nuclear Materials in the MICADO Project. Sensors 2021, 21, 2630. https://doi.org/10.3390/s21082630

2/8 MICADO Project. Available online: https://www.micado-project.eu/ (accessed on 30 Nov 2023).

2/9 Luxium Solutions (previously Saint Gobain Crystals) scintillating fibers. Available online: https://www.mi-net.co.uk/product/scintillating-fiber/ (accessed on 14 Dec 2023).

2/10 ON Semiconductor. Available online: https://www.onsemi.com/products/sensors/photodetectors-sipm-spad/silicon-photomultipliers-sipm (accessed on 4 Dec 2023).

2/11 Dolgoshein, B.; Balagura, V.; Buzhan, P.; Danilov, M.; Filatov, L.; Garutti, E.; Groll, M.; Ilyin, A.; Kantserova, V.; Kaplin, V.; et al. Status report on silicon photomultiplier development and its applications. Nucl. Instrum. Meth. A, 2006, 563, 368.

2/12 Zappa, F.; Tisa, S.; Tosi, A.; Cova, Principles and features of single-photon avalanche diode arrays. S. Sens. Actuators A, 2007, 140, 103.

2/13 Finocchiaro, P.; Pappalardo, A.; Cosentino, L.; Belluso, M.; Billotta, S.; Bonanno, G.; Carbone, B.; Condorelli, G.; Di Mauro, S.; Fallica, G.; et al. Characterization of a Novel 100-Channel Silicon Photomultiplier—Part I: Noise. IEEE Trans. Electron Devices, 2008, 55, 2757.

2/14 Finocchiaro, P.; Pappalardo, A.; Cosentino, L.; Belluso, M.; Billotta, S.; Bonanno, G.; Carbone, B.; Condorelli, G.; Di Mauro, S.; Fallica, G.; et al. Characterization of a Novel 100-Channel Silicon Photomultiplier— Part II: Charge and Time. IEEE Trans. Electron Devices, 2008, 55, 2765.

2/15 Fasso, A.; Ferrari, A.; Ranft, J.; Sala, P.R. FLUKA: A Multi-Particle Transport Code; CERN Technical Report No. SLAC-R-773; Stanford University: Stanford, CA, USA, 2005.

3 Sensorised LoRa Wireless Sensor Network for Identification and Integrity Assessment of Radioactive Waste Drums

Andrea Chierici, Rosa Lo Frano, Riccardo Ciolini, Francesco d'Errico,
Department of Industrial and Civil Engineering, University of Pisa, 56122 Pisa, Italy

3.1 Background

Radioactive waste from nuclear activities requires secure packaging for safe disposal in line with global standards. Technological advances now allow for the use of wireless sensor networks (WSN) for long-term waste monitoring, reducing dependence on complex cables or scanning systems. This method decreases inconsistencies and human errors in package management during disposal, and integration with decommissioning machinery enables real-time radiation data collection throughout the whole disposal process.
The University of Pisa (UniPi) developed, tested, and validated an innovative platform to assess waste form durability in repository conditions, both operational and post-closure, as part of T7.3's focus on sensing technology. The prototypes were tested in labs and actual storage sites, tailored for complex facilities with potential issues like limited internet and structural attenuation. Its versatility enhances its use across standard and complex waste package geometries.
Utilizing passive gamma and neutron counting, this method targets the long-term monitoring of radiological levels in radioactive waste drums (RWDs) to evaluate surface radiation intensity and internal structural integrity. By examining fluence variations over time, the goal is to identify structural changes in the waste matrix autonomously, minimizing the inconsistencies and human errors common in waste package management during disposal.

Keywords: LoRa, Sensor Networks, Gamma-ray and Neutron Detection, Non-Destructive Techniques, Long-Term Monitoring

3.2 Method

The proposed WSN consists of three integrated levels (Figure 1). The first layer consists of LoRa Nodes responsible for package identification and radiation data collection from within the waste package, aiding in the monitoring of the waste drums' structural condition. The second layer, LoRa Gateways, handles the LoRa traffic and forwards the data to local storage or e.g. an Azure IoT Central application via Wi-Fi, employing a Message Queuing Telemetry Transport (MQTT) broker. These gateways also synchronize all nodes using acknowledgment radio payloads to prevent data transmission collisions. Finally, the third layer is a Cloud-based platform, implemented through an Azure IoT Central application, facilitating remote access and data processing.

Data is presented on interactive dashboards for easy analysis, with metadata detailing network components such as sensors, nodes, and gateways. This platform allows remote access to the sensor network, although the network remains operational even without internet connectivity.

Long-range radio (LoRa) technology was selected for wireless communication due to its low energy consumption, cost-effectiveness, and superior transmission distance, effective even through large obstacles. Moreover, the decentralized nature of LoRa improves data handling efficiency, reducing reliance on constant centralized or cloud-based connections, a critical aspect in environments like

radioactive waste storage or nuclear power plants where consistent network availability is challenging.

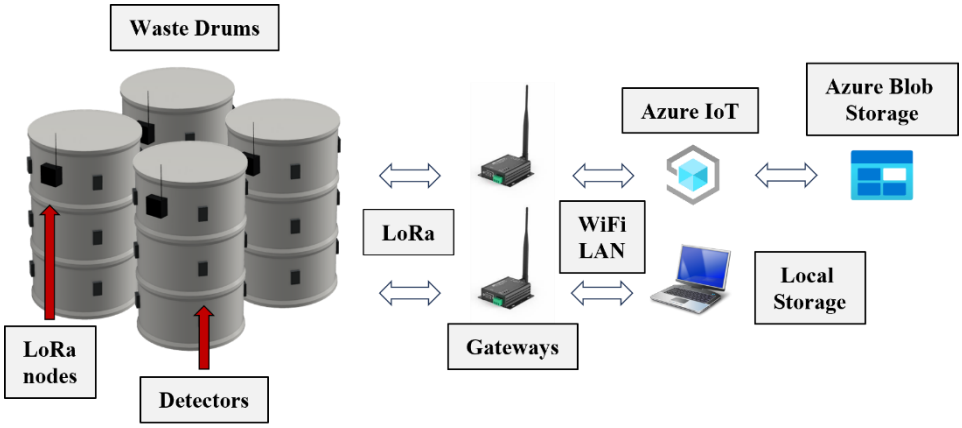

Fig. 1 Radiation monitoring framework for radioactive waste drums.

3.3 Technical Development

The wireless sensor nodes at the heart of the system combine a high-precision, temperature-compensated Real Time Clock (RTC) with a power-efficient microcontroller (MCU) for task scheduling and operations control. For communication, nodes utilize UART-interface LoRa transceivers (based on the LLCC68 chip from Semtech) capable of wake-on radio functionality, which allows them to conserve energy by remaining in a sleep state until triggered by incoming radio signals.

Operational tasks and data transmission timings are managed by the RTC, with nodes mainly in energy-saving mode to prolong battery life. The system uses time-division multiple access (TDMA) and listen-before-talk (LBT) for efficient communication. RTC recalibration and an integrated MCU RTC ensure precise timing and system integrity. In case of malfunctions, the system's state is saved before a reset by the Watchdog Timer (WDT), preserving data and reliability.

Radiation data is captured during predetermined intervals, known as measure windows, which can be fine-tuned for their occurrence and length to balance power efficiency, data detail, and measurement precision. After the designated number of measure windows, the system transmits the collected data. Moreover, if the radiation fluence surpasses a predefined threshold, the system promptly raises an alert and conducts an expedited data transmission.

Within this system, each node is engineered to support up to eight, micro-power gamma ray and thermal neutron detectors in parallel. For gamma-ray detection, BG51 detectors from Teviso (Switzerland) were chosen, which utilize a modified silicon PIN diode array as its sensing element. For thermal neutrons, Domino v5.4 detectors from Radiation Detection Technologies (USA) were employed, incorporating a Microstructured Semiconductor Neutron Detector (MSND) technology that combines a 6Li converter with silicon diodes.

In the WSN, LoRa gateways, powered by an Espressif ESP32 MCU, are tasked to handle data reception from nodes, send ACKs, and maintain the accuracy of node clocks to ensure precise measurement and transmission schedules. Received data is locally preserved on SD cards and concurrently sent to an Azure IoT Central application.

The system's cloud infrastructure supports customized monitoring dashboards through the addition and configuration of nodes. This allows for advanced data management and presentation, with minimized human error due to the system's automated processes, ensuring a reliable radiation monitoring workflow.

Currently, the prototypes are at a Readiness Level of at least 7, since they were installed, tested, and validated in an operative environment (a real waste storage site).

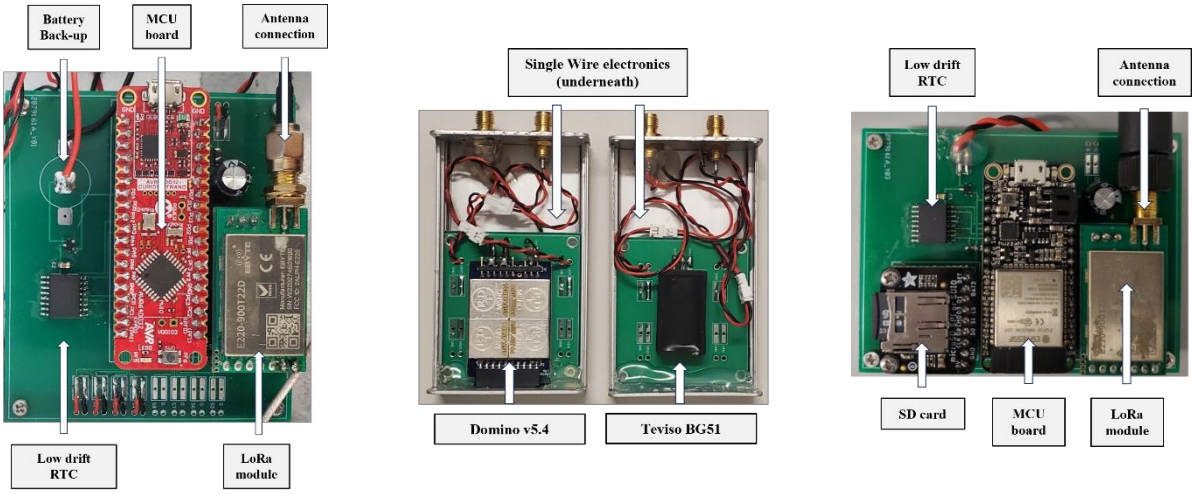

Fig. 2 Prototypes of the LoRa node (left), single-wire detectors (middle), LoRa gateway (right).

3.4. Lab Tests

Initial testing to investigate the functionality of the sensorised LoRa nodes was conducted at the University of Pisa's Laboratory of Nuclear Measurements (LNM). This stage involved verifying the sensitivity and efficiency of the detectors, together with the long-term reliability of the system in executing tasks like data acquisition, data transmission, and the cycling between active and deep-sleep states.

For the evaluation, the integration window ΔT for all detectors was established at 1 hour, with a repetition period of 6 hours. Over a month's worth of background radiation data was utilized to estimate metrics such as the minimum detectable count rate (MDCR) and minimum detectable fluence rate (MDFR).

Subsequently, a 140.4 kBq Cs-137-pointlike source was used to expose the gamma-ray detectors stationed atop an unoccupied aluminum support, and a 1.1 GBq Am-Be neutron source, moderated with 25 cm of PMMA, was used to produce a measurable thermal neutrons fluence rate (up to 0.5 eV) of 100 ± 12 cm^{-2} min^{-1} in the air at 25 cm from the source itself (Figure 3 and Figure 4).

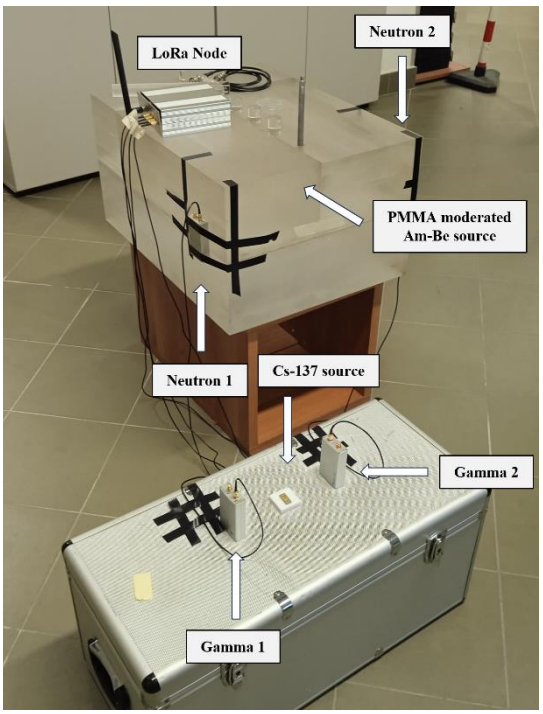

Fig. 3 LNM measurements setup.

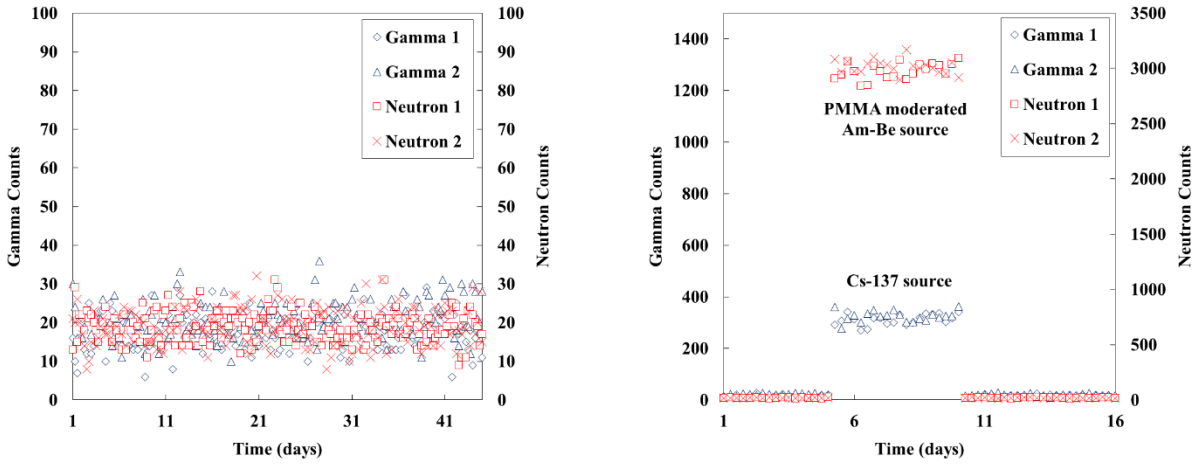

Fig. 4 Data collected by the LoRa node in absence (left) and in presence (right) of the sources.

The results align with the manufacturer's specifications that cite a sensitivity for gamma detectors equal to 5 (± 15%) CPM/µSv/h at 662 keV, and an efficiency of up to 30% for thermal neutrons (Table 1). Additionally, no significant discrepancy was observed between the tested detectors.

Table 1 Summary of the characterization of the detectors conducted at the LNM of UniPi.

Detector ID	Efficiency (%)	Sensitivity (CPM/µSv/h)	MDFR (n cm^{-2} min^{-1})
Gamma 1	0.18 ± 0.01	5.2 ± 0.3	522.8 ± 26.5
Gamma 2	0.18 ± 0.01	5.2 ± 0.3	588.7 ± 29.2
Neutron 1	13.0 ± 0.3	757.9 ± 6.5	1.01 ± 0.03

Neutron 2	13.1 ± 0.3	759.7 ± 6.5	1.02 ± 0.03

Notes: MDFR = Minimum Detectable Fluence Rate

The LoRa node was also tested for electrical power consumption, communication efficiency under NLOS conditions, and EMI immunity. Its power consumption was notably low, averaging 15 µA, and even less during deep sleep mode. Communication tests revealed strong transmission capabilities over 250 meters in NLOS scenarios; additionally, the node's performance remained stable amidst high-power radio transceivers, indicating robust EMI resistance.

3.5. Test in a Realistic Environment

3.5.1. Installation in Nucleo Storage site

The initial testing phase was followed by the system's deployment and assessment at the Nucleco interim radioactive waste storage facility in Rome, Italy. A LoRa node equipped with two gamma and two thermal neutron detectors was mounted on a 380 L cemented overpack containing sources with a total activity exceeding 100 GBq of Am-Be and 9 GBq of Cs-137. Owing to the high radiation emitted by the cemented package, the measurement schedule was set to every hour with a 12.5-minute integration period. The selection of the integration period aimed to attain a detectable ambient equivalent dose rate of approximately 0.2 µSv/h for gamma detectors, factoring in their constrained sensitivity and efficiency as determined by prior testing. The system recorded data over 19 hours on the overpack, and to ensure thorough coverage and account for any uneven distribution of material within the container, the four detectors were placed at equal intervals of 90 degrees around it (Figure 5).

Importantly, the experiments validated the device's capability to transmit data through four buildings filled with cemented waste drums without repeaters and to the Azure IoT Central application for remote processing and control. Variations in count rates between similar detectors were ascribed to the uneven composition of the concrete and the spatial arrangement of the sources, corroborated with reference detectors provided by the LNM (Figure 6).

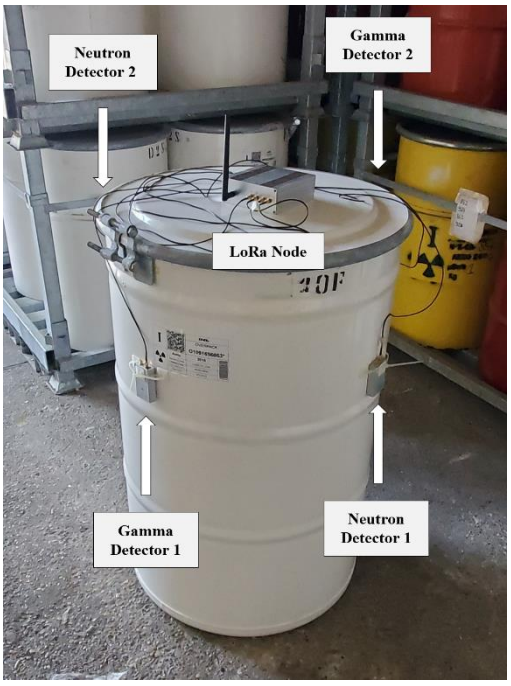

Fig. 5 LoRa node installed on a cemented 380 L overpack.

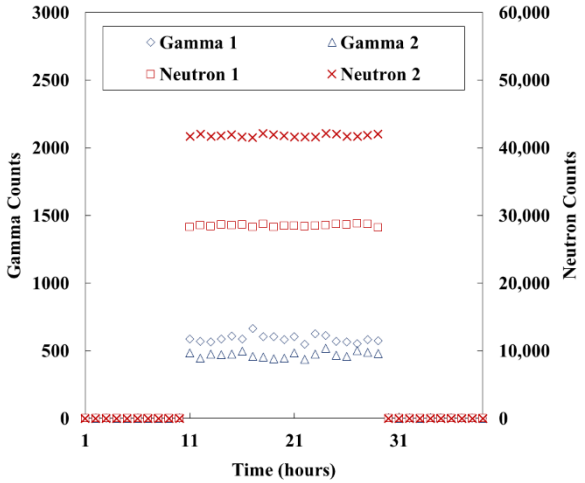

Fig. 6 Data collected from the wireless node placed on the 380L cemented overpack in the Nucleco storage site over 19 hours.

The gathered data highlights the feasibility of identifying variations in activity or structure within the container, especially using several linked detectors to improve the coverage of the drum. Thus, implementing a system of these devices in a radioactive waste storage site could provide a means for automated, remote, and long-term radiological surveillance, benefiting from its low power usage.

3.5.2. PREDIS Joint Demonstration Test

To the goals of Task 7.6 of the PREDIS project, a collaborative demonstration test was conducted to assess the long-term effectiveness of technologies developed by the involved participating partners. The test took place at the Nuclear Research Institute Rez (ÚJV Řež, a.s.) in the Czech Republic.

At ÚJV Řež, the test involved the use of standard 200 L drums (model 0485, 820 mm in height, 1.2 mm thick galvanized steel), to replicate the conditions found in typical real-world waste storage facilities. A dedicated mock-up, designed for radiological experiments, was created: this mock-up featured a 2.5 cm lateral gap and a middle opening to house a Cs-137 source of 167 MBq secured within a steel container measuring 5.2 mm in width and 15.9 mm in height.

In the experiment, a LoRa node, with four gamma detectors numbered 1 through 4, and two thermal neutron detectors, numbered 1 and 2, was attached to the active mock-up. The gateway, linking to a Wi-Fi network, was in a data equipment area (DEA) two floors up from the storage location. Data capture was programmed to occur every hour for testing purposes, with gamma detector active for 12.5 minutes per hour, and thermal neutron detectors for 1 minute each hour, based on their documented efficiency and sensitivity from previous studies. The arrangement of the detectors around the closed drum is shown in Figure 7, where the expected theoretical Monte Carlo computed ambient dose equivalent rate at the gamma measuring points is also depicted. The configuration of the detection points was as follows: Gamma detector 1 was positioned at 0 degrees directly in front of the slot, while Gamma detectors 2 through 4 were placed at 90-degree intervals moving anticlockwise. Neutron detectors 1 and 2 were situated at 45-degree angles, with Neutron detector 1 between Gamma 1 and Gamma 4, and Neutron detector 2 between Gamma 3 and Gamma 2.

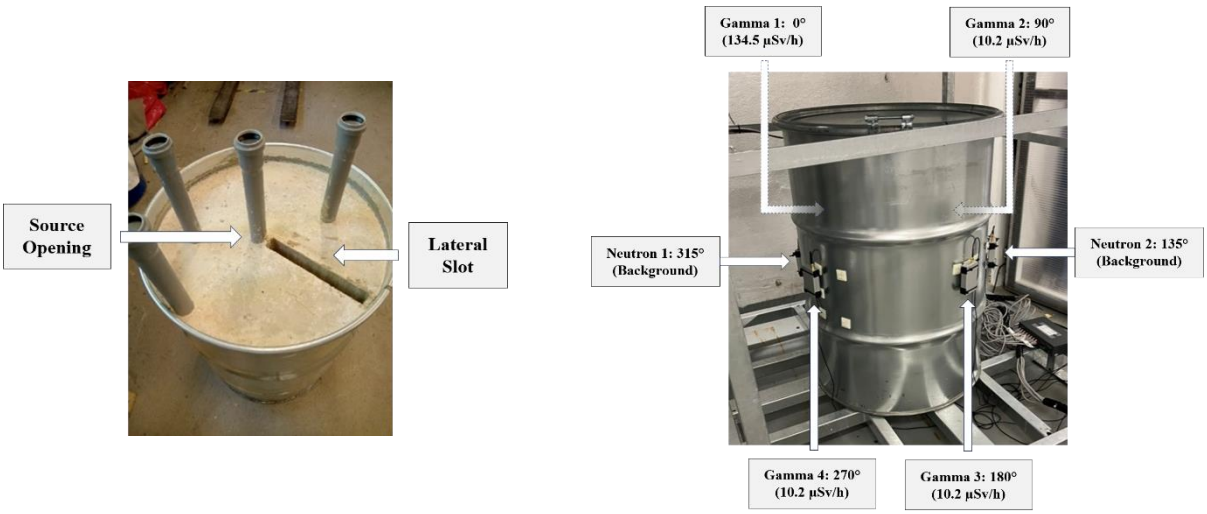

Fig. 7 Construction of the active mock-up featuring a 2.5 cm side gap and multiple openings for housing radioactive sources (left). Installation of gamma and neutron detectors on the drum's metallic mid-section (right).

The objectives of the test encompassed several aspects, starting with verifying the accuracy of radiation intensity measurements by the detectors, test the effectiveness of wireless data transmission in environments lacking internet connectivity, and assess the battery's longevity. Additionally, the test aimed to evaluate the system's ability to detect signs of structural integrity loss, indicated by increased radiation fluence, using the lateral slot as a defect.

Figure 8 displays data collected across a span exceeding 3 months, where count rates have been transformed into ambient dose equivalent rates using a calibration factor for Cs-137 derived from previous tests. The data for thermal neutrons predominantly indicate background levels.

Three months into its operation, the system experienced a 15% reduction in battery life, however, by reducing the frequency of measurements from the original hourly schedule, the system's battery life could be substantially prolonged, also decreasing power usage.

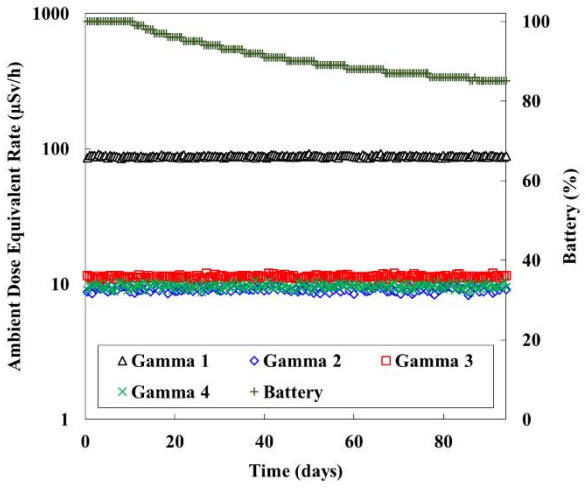

Fig. 8 Data spanning over three months show the gamma detector, positioned directly opposite the slot, detecting a higher dose rate than the remaining three detectors.

3.6. Summary and Outlook

UniPi designed and developed a novel technology for monitoring the structural integrity of stored RWDs using wireless sensor nodes for automated, remote data collection. The system, leveraging

LoRa technology for its low energy, cost-efficiency, and long-range capabilities, underwent initial characterization at the LNM of UniPi, and subsequently underwent field trials at the Nucleco site in Rome and a three-month demonstration at ÚJV Řež as part of the PREDIS project. These tests validated the technology's capability for detailed activity monitoring and anomaly detection within containers, emphasizing its suitability for remote, automated monitoring without internet connectivity. Key aspects assessed included the accuracy of radiation detectors, wireless data transmission reliability, battery life, and the system's ability to detect structural changes within the drum's matrix, proving its effectiveness for long-term RWD surveillance and its adaptability to different operational needs.

The platform's durability is under evaluation through radiation hardness tests for its applicability in managing low to intermediate-level radioactive waste. This includes studying material aging and other factors that influence detection accuracy and effectiveness. Furthermore, the economic and regulatory feasibility of the technology is being analyzed to ensure its cost-effectiveness and sustainability. Efforts are also being made to improve data management with the creation of intuitive dashboards and analytical tools for enhanced decision-making by users and stakeholders. Moreover, research into standalone units with LoRa transceivers is underway to remove the reliance on wired connections. This is complemented by advancements in sensors capable of identifying various gamma energy levels, facilitating edge computing for immediate integrity analysis while accounting for gamma emitter decay, thus refining waste drum monitoring techniques.

4 Acoustic Emission for measuring ASR

Gert Dekkers and Dylan Gybels
Magics Technologies

Abstract

Alkali-silica reaction (ASR), and the subsequent formation of a gel-like product, may destabilize the waste form. Swelling of the gel leads to stress development and potential cracking of the concrete. To assess the integrity of the barrel, non-destructive monitoring is of interest. To this end, acoustic emission (AE) is considered. AE uses highly sensitive piezoelectric sensors to record the elastic stress waves emitted during the formation of cracks. Although research indicates a clear correlation of AE and ASR, it has not been demonstrated on barrels containing nuclear waste. This report will introduce the measurement prototypes and its experimental tests.

Keywords: Acoustic Emission, data collection, data analysis

4.1 Background

Pre-disposal waste management aims to create suitable waste packages for storage, transport, and final disposal. Cement-based materials (CBM) have been extensively used in the nuclear industry for this purpose due to their simplicity, low cost, and advantageous properties like self-shielding and high alkalinity. However, issues such as gel formation due to alkali-silica reaction (ASR) have been observed, disrupting the stability of waste forms. ASR, a harmful reaction between silica and alkalis in the presence of water, leads to gel formation and concrete degradation, influenced by various factors including temperature, material composition, and aggregate characteristics. Additionally, irradiation can increase the reactivity of silica-rich aggregates, further impacting concrete properties. Swelling of aforementioned gel leads to stress development and potentially, cracking of concrete. To monitor this behaviour in a non-destructable manner, a technology is explored that can detect these cracks by means of capturing acoustic waves in the concrete.

4.2 Method

When a crack occurs, the elastic stress wave propagates through the material which could be recorded by an AE sensor. To detect such AE events, processing is needed on the continuous waveform. Given the detected events, a cumulative event count will be generated in function of time as shown in Fig. 1.

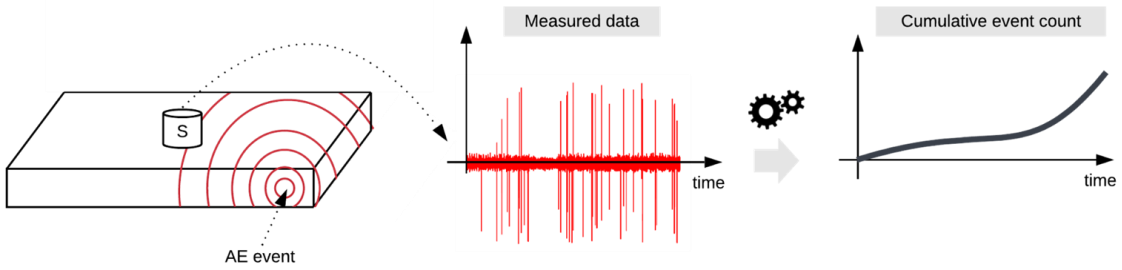

Fig. 1: Acoustic emission concept

4.3 Technical development

To validate the AE technology within this application, off-the-shelf components are used throughout all experiments. Our experimental setup (see Fig. 2) consists out of a Physical Acoustics R15a piezo electric sensor, Mistras 2/4/6 pre-amplifier, PicoScope 5000 analog-to-digital converter and a data logger to store the collected waveforms. An algorithm was designed that can detect the AE events for which a cumulative event count graph can be generated.

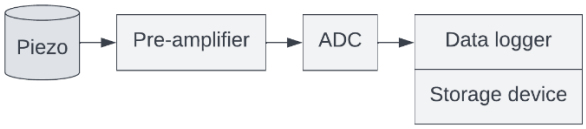

Fig. 2: Prototype

Although this set up serves its purpose for collecting data, it's not necessarily sufficient to perform experiments for a long duration. Hence, depending on the experiment duration different setups were generated to accommodate for a higher reliability and ease of use.

4.4 Lab tests

The goal of the data collection campaign is two-fold, as indicated by Figure 3. On the one hand, it's aim is to validate the AE sensor as a viable NDT method to assess the integrity of barrel. Secondly, the data will also be used to validate a digital twin model. In complement to sensors, the digital twin model aims to predict the integrity. Hence, both methodologies are complementary such that it makes sense to validate these holistically. Concerning the data collection, both a lab as drum-scale experiment is conducted. The lab-scale experiments are used for preliminary validation of AE and to calibrate the digital model. The drum-scale experiment is meant for real-scale validation of both approaches.

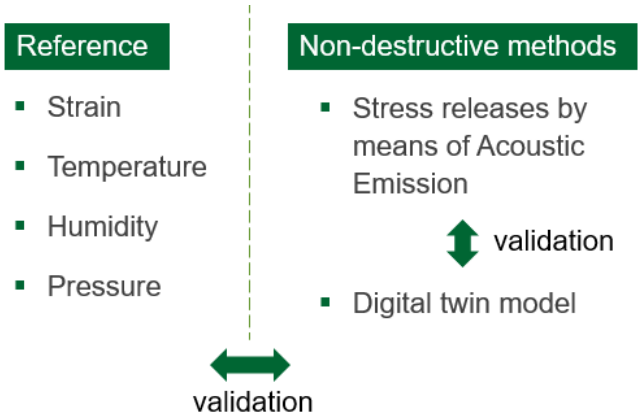

Fig. 3: Prototype

Two lab-scale test campaigns have either been carried out or are ongoing. These experiments were conducted not only to validate AE technology, but also to verify and construct a digital twin model (Task 7.4).

4.4.1 Setup

The first and second lab-scale experiment was performed in an accelerated environment. Three concrete samples of size 25x25x285 mm were equipped with AE sensors in accelerated conditions for a duration of 28 days. All samples are mixtures of Portland cement with a (non-)reactive aggregate. The first two samples contain Sibelco sand (non-reactive) or River sand (reactive) and are denoted as *Sib1* and *Riv3* in Fig. 8 the respectively. Regarding the third sample, the same composition as Riv3 is used but with the addition of LiNO3 to mitigate ASR. An example of a sample is shown in Fig. 4.

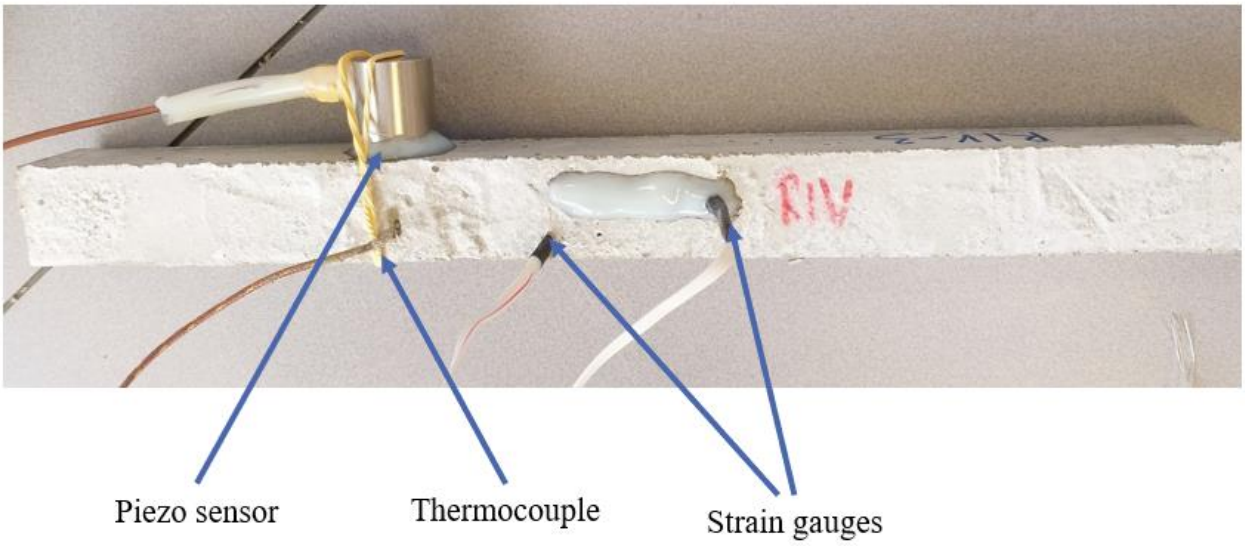

Fig. 4: A sample equipped with an AE sensor, thermocouple and strain gauge

Concerning the first lab-scale test, its intent was to evaluate the measurement setup in a highly accelerated environment as shown in Figure 5. The mortar bar samples were placed in a high temperature chamber at 80 °C for a duration of a month.

Fig. 5: Mortar bar placement in a high temperature chamber, at 80 °C, for a duration of 1 month

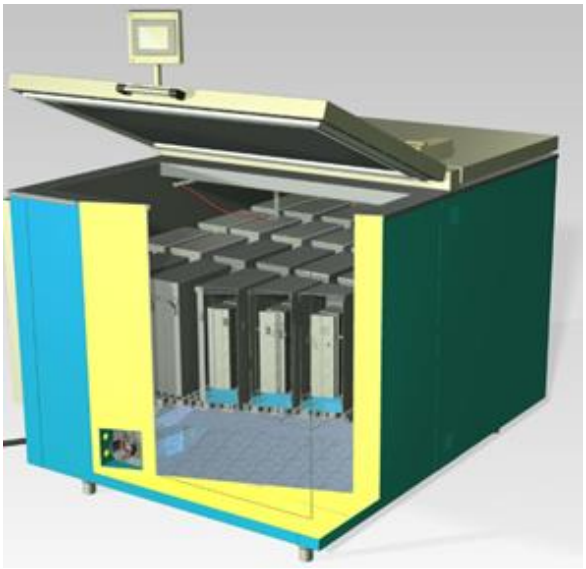

Fig. 6: Mortar bar placement in a typical industrial ASR chamber, at 38 °C, for a duration of 1 year

As a reference, strain gauges were applied to the sample and manual measurements of mass and length were conducted periodically. More information on the measurement setup can retrieved at (Phung, et al., 2021). Throughout the experiment, multiple impulsive events were observable in the recorded waveforms such as in Fig. 7.

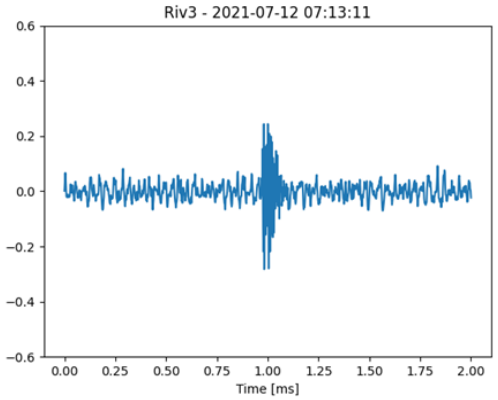

Fig. 7: Example of an AE event for a reactive sample

4.4.2 Results

Concerning the first lab-scale experiments, the cumulative event plot of the AE events indicated a clear correlation with the measurement of the strain gauges and the manual measurements (Phung, et al., 2021) as shown by Fig. 8. The most reactive mixture (*Riv3*) in terms of ASR clearly shows more AE events and expansion with respect to the other samples. Interestingly, the addition of LiNO3 (*Li1*) shows to significantly reduce ASR activity.

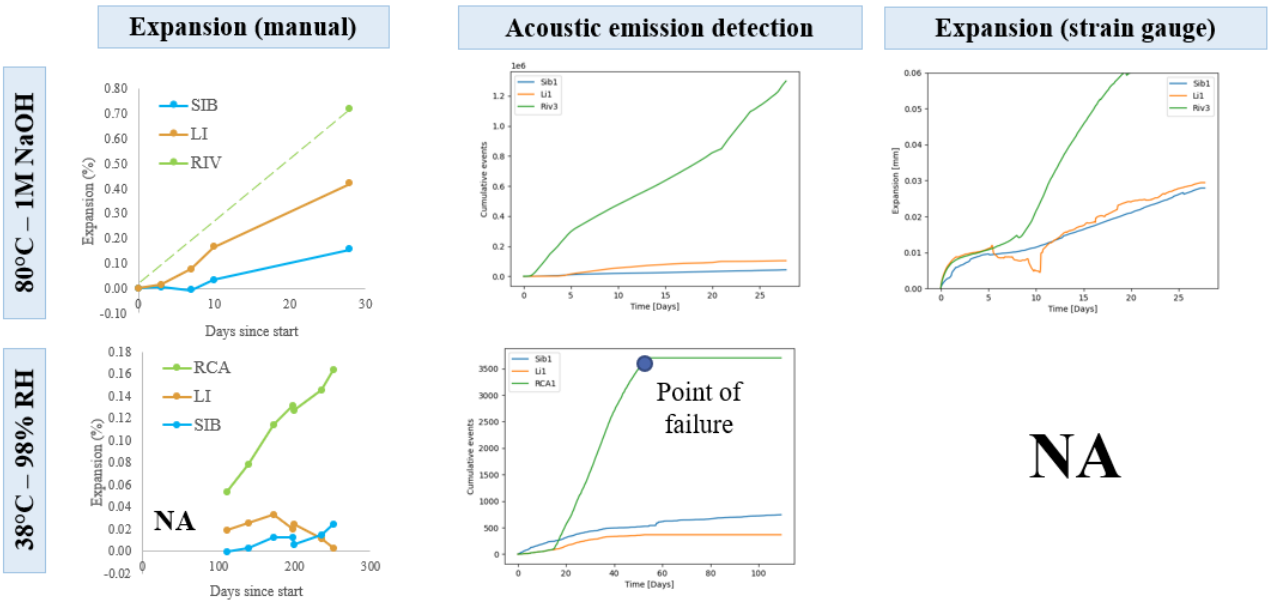

Fig. 8: Expansion measured by strain gauges (left) along with the cumulative event count by means of AE (right)

During the second lab-scale experiment, multiple sensor failures we're experienced. The strain gauges contained data with a high amount of variation, and no clear correlation between the manual measurements. Secondly, during the replacement and inspection of these strain gauges, one of the AE sensors failed. Our hypothesis is that the contact between the material and the AE sensor was compromised leading to a different amplitude distribution. As detection of AE events relies on threshold-based detection, a change in the coupling between the two can have a significant impact.

To avoid having the same issues on the drum-scale experiment, a different mounting strategy was selected for the AE sensors. Secondly, instead of strain gauges, industry-grade vibrating strain wires were used that are more robust in these harsh environments. Hence, given these changes it was assumed that we could reliably conduct the drum-scale experiments.

4.5 Test in a realistic environment

4.5.1 Experimental setup

AE is shown to correlate well with expansion on lab-scale. Before moving on towards nuclear waste drums, the next step was to evaluate it on drum-scale given similar concrete mixtures that have been used at lab-scale. Hence, a similar concrete mixture is used without any nuclear waste. Specifically, the RCA and Sib recipes were re-used for this experiment. The recipes were used to cast 4 drums of which 2 drums were placed in a temperature-controlled chamber set at 38 °C to accelerate the ASR. The other 2 drums were tested under ambient temperature, which are monitored during the test as shown by Figure 9.

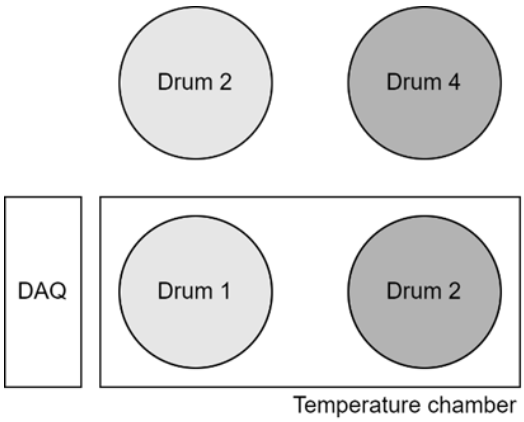

Fig. 9: Overview of the conceptual setup. In total 4 drums were equipped with multiple sensors.

These drums of 885mm height and ±600mm diameter were each be equipped with 2 AE sensors, 8 vibrating strain wires, 1 pressure sensor and 1 humidity sensor. Two different concrete mixtures used and placed in either accelerated or non-accelerated conditions.

Fig. 10: Real-life barrel (left) and drawing of the supporting structure for the vibrating strain wires and thermistors (right)

Figure 10 shows the barrel on the left, with a CAD design of a supporting structure to hold the sensors in-place at the right. Due to boundary conditions of the steel barrel, the mixture will not have uniform behaviour during swelling and shrinking. Hence, the sensor locations were carefully chosen based on an analytical model provided by SCK-CEN to maximise the information gain. Figure 10 shows the supporting structure after it's placed inside the barrel. It supports 8 sensors that contain a vibrating strain wire and thermistor.

Fig. 11: Support structure with mounted sensors

The relative locations for each of the vibrating strain wire and temperature sensor are identical for each drum and are provided in Figure 8-7. For additional clarity, the relative coordinates with respect to the bottom and centre of the barrel are provided in Table 2. Note that Figure 8-7 shows X and Z. Dimension Y is identical (Y=0) for each sensor location.

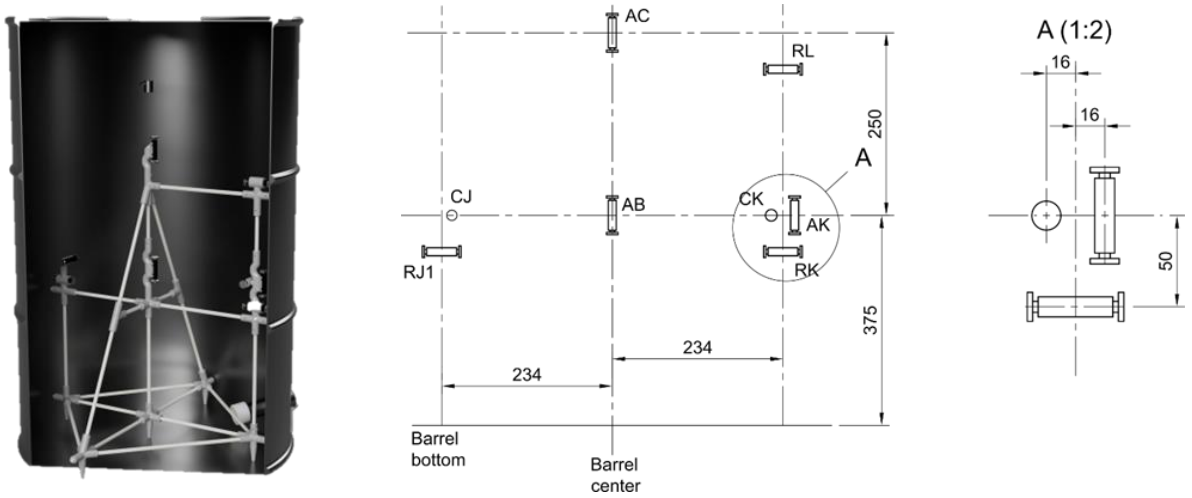

Fig. 12: 3D render of the PLA structure inside the drum (left) and the schematic concerning relative positioning of each sensor (right).

Table 2. Sensor location per barrel relative to the bottom and centre of the barrel

Sensor identifier	X (mm)	Y (mm)	Z (mm)
CJ	-218	0	375
RJ	-234	0	325
AC	0	0	625
AB	0	0	375
RL	234	0	575
CK	218	0	375
AK	250	0	375
RK	234	0	325

Concerning AE, a sensor is mounted inside the drum on top of the concrete, and one outside the drum. Concerning mounting it was opted for a holder that's either screwed to attach with the concrete or magnetically placed, as shown Figure 12. To ensure acoustic coupling, an EA 9466 epoxy was applied. Additionally, Figure 12 shows some pictures of during the casting process.

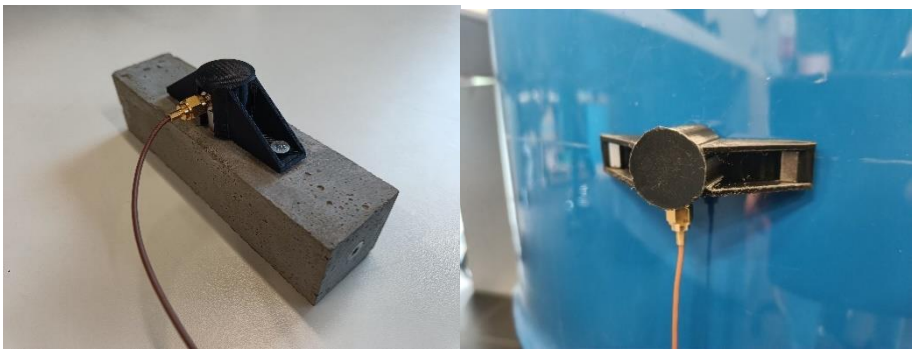

Fig. 13: AE sensor placement on top of the concrete (left), and attached to the barrel (right)

Fig. 14: Casting process

Once all the barrels were casted, the heating belts were turned on. The following image shows the temperature chamber, along with two barrels, heating belts and some sensors.

Fig. 15: Temperature chamber

As the experiment will be conducted for 2 years, additional measures are needed to do this reliability. For this purpose, dashboard and alerting have been added to the prototype shown in Figure 15. As such, the following logging architecture was set up.

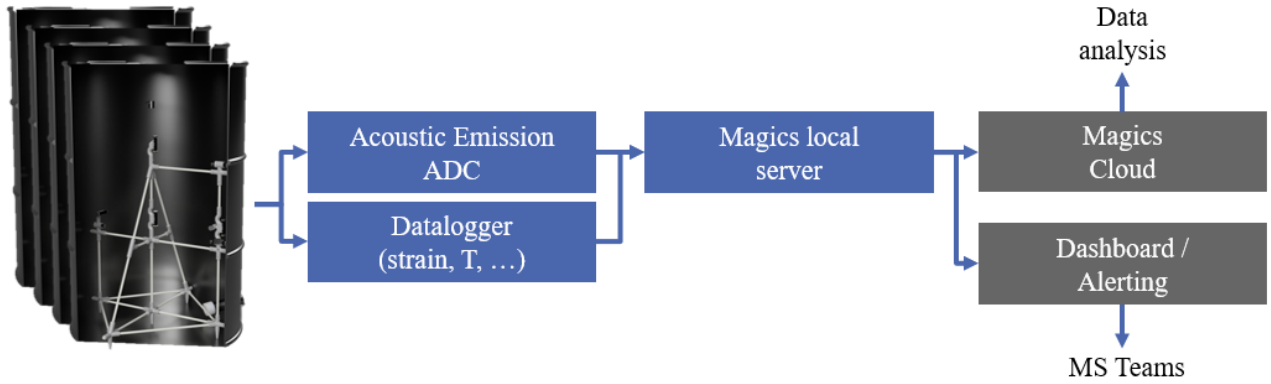

Fig. 16: Logging architecture

Experiments were conducted at a remote location. The data was scraped from the local server, from our cloud to offer reliable storage, dashboards and alerting. During the lab-scale experiments it was clear that this was needed. The alerting service is set such that it notifies us directly in case of an infrastructural error or if the statistics of the data are diverging from the norm. Additionally, the dashboard provided convenient manual inspection which had proven to be useful especially at the start of the measurement campaign. The dashboard can be accessed via https://34.140.215.210/ (user: guest, password: magicstech).

Concerning data acquisition of the vibrating strain wires, multiple multiplexers, frequency analysers and DAQ's were used from Campbell.

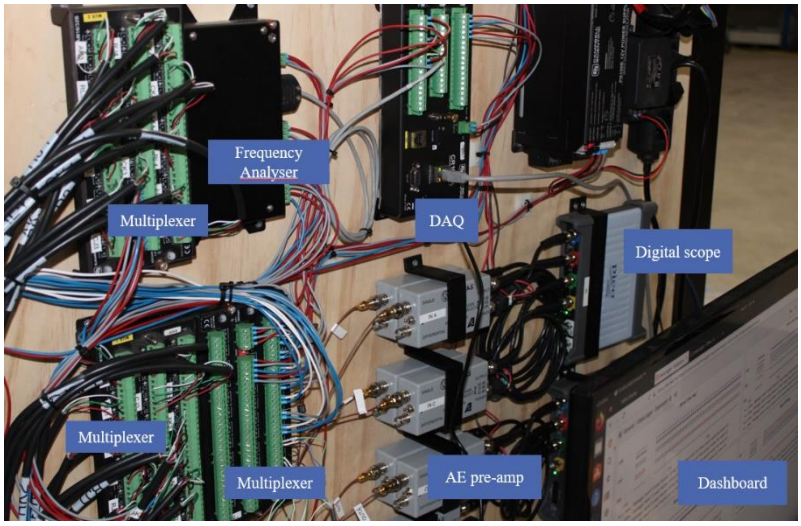

Fig. 17: Data acquisition setup

4.5.2 Results

To evaluate the technology, a reliable reference is of importance. Unfortunately, results of this reference have shown to have inconsistent results. The prior sensor modality to compare AE to is the relative strain present in the concrete. However, as the vibrating strain gauge measures a resonant frequency, a transformation is applied to transform the resonance frequency to relative strain. As these sensors are also temperature dependent, a temperature compensation was applied as well. These transformations are conformed with the manufacturer's datasheet (RocTest). Figure 18 shows the temperature evolution of each barrel for first year of the experiment. The temperature

of the ambient barrels (2 and 4) clearly follows the ambient temperature, while the ones in the controlled chamber are relatively static.

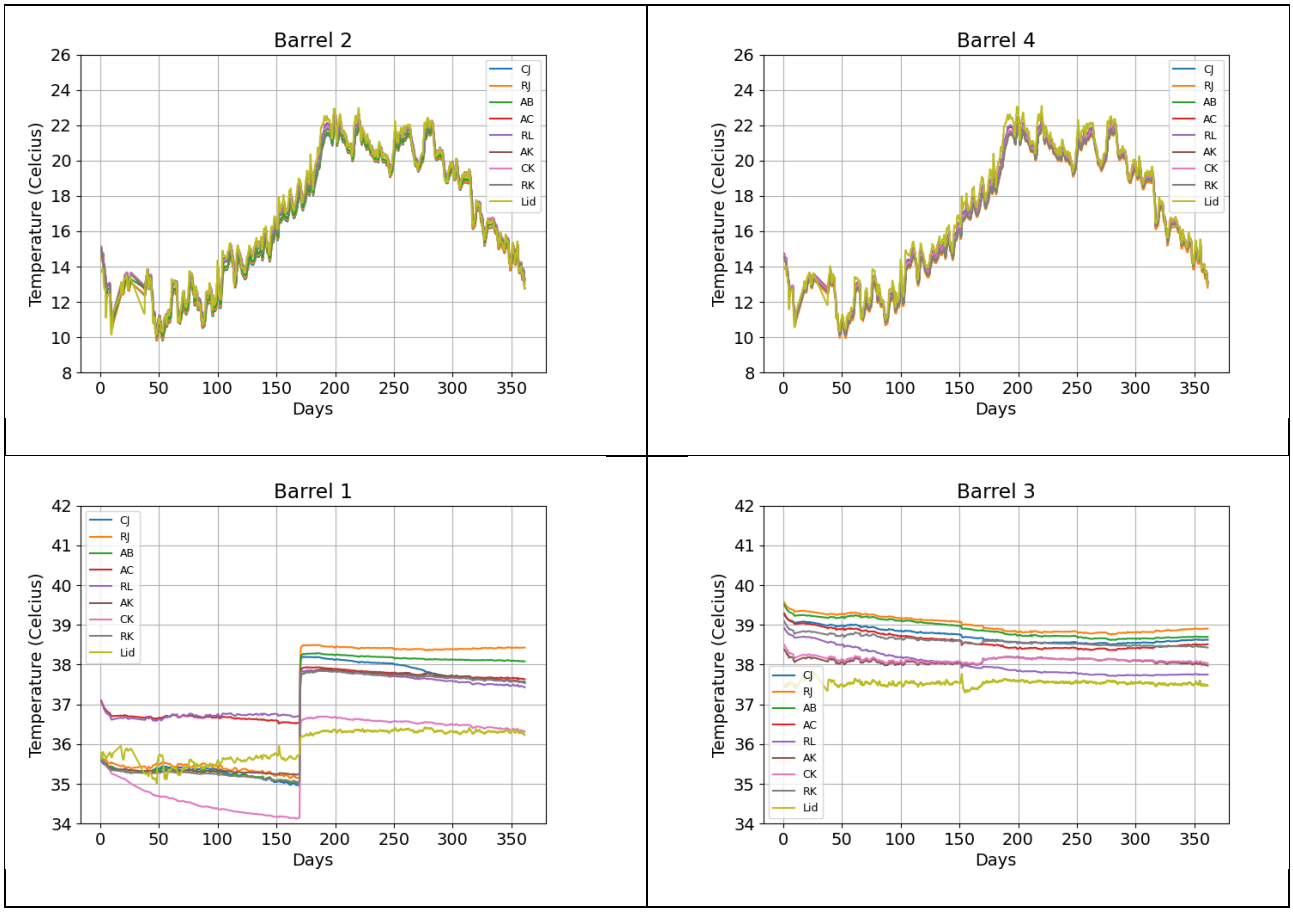

Fig. 18: Data acquisition setup

Figure 19 shows the relative strain in function of time. From a first perspective, it's clear that the analysis of these graphs is not straightforward. There are a multitude of explanations for this:

- A few sensors seem to have unrealistic strain measurements (e.g. AB1 and AC1. In that sense that these exceed the predicted maximum gradient of the relative strain. It is assumed that the flanges of the strain gauges have poor contact with the concrete due to limited concrete in-between the flange and the structure.
- Temperature dependencies that were not entirely removed due to the temperature compensation that was applied.
- No expansion has been observed so far, while this was initially expected. There are currently on-going additional lab-scale tests by SCK-CEN to confirm why this is not happening.
- As no clear expansion is occurring, the variation in observed strains could be potentially attributed to difference in location in the concrete, mounting and casting.

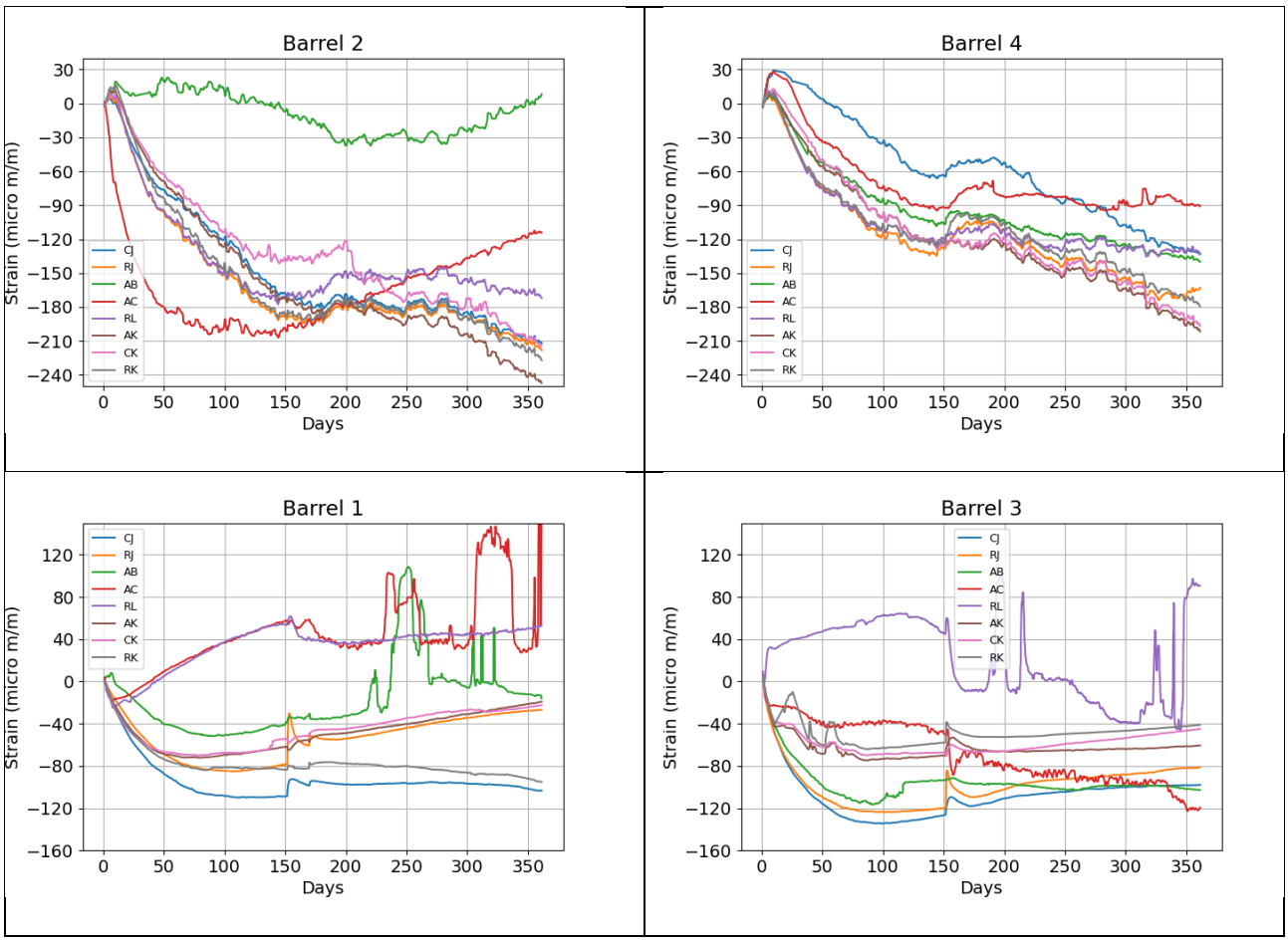

Fig. 19: Data acquisition setup

The fact that there currently is no expansion ongoing, along with the high variability in the observed strain led to the conclusion that it was currently deemed to be highly impractical to proceed with the analysis of the AE.
It was decided to let the experiment continue till the end of the project and then re-evaluate whether to process the data. Focus for the coming months will be on identifying what could be improved to the drum-scale experiment to improve the reliability of these reference measurements.

4.6 Summary and outlook

The applicability of Acoustic Emission has been shown in the context of lab-scale experiments. Preliminary experiments indicate a correlation between cumulative acoustic events and expansion for the selected concrete mixture and environmental conditions. However, a distinctive expansion has not been observed yet on the drum-scale experiments. Hence, it was decided to delay the processing and analysis of the collected AE data till a change is observed.

4.7 References

Johann, S. e. (2017). RFID sensor systems embedded in concrete–Validation experiments for long-term monitoring. The e-journal of nondestructive testing & ultrasonics, Artikel-8.

Phung, Q. T., Frederickx, L., Nguyen, T. N., Seetharam, S., Laloy, E., Verbeeck, J., . . . Valgaeren, C. (2021). An integrated approach to assess the alkali silica reaction of cemented wastes . *Predis Workshop 2021*, (pp. 94-106).

RocTest. (n.d.). Instruction manual. embedded strain gauge, Model EM-5. Retrieved from https://roctest.com/wp-content/uploads/2017/01/E10114-060220_EM-Serie.pdf

Strangfeld, C., Johann, S., & Bartholomai, M. (n.d.). Smart RFID Sensors Embedded in Building Structures for Early Damage Detection and Long-Term Monitoring.

5 Ultrasonic Inspection

NNL Reference: EU11726/06/10/04
Omer Elnasaney, National Nuclear Laboratory
Darren Potter, National Nuclear Laboratory

5.1 Background

This chapter proposes the use of non-contact air-coupled ultrasonic transducers to inspect the ILW drums. The non-contact air-coupled ultrasonic transducers can provide circumferential measurements to detect swelling in the drums and provide screening for discontinuity defects such as cracks or corrosion cavities. The ultrasonic signals used in the measurements can also provide an indication of the pressure build up inside the drums, possibly indicate the content moisture. The air-coupled ultrasonic inspection can be performed on legacy containers without any modification to the containers or their storage arrangement, making it ideal for in-situ inspection inside storage vaults. To perform the circumferential measurements, a longitudinal ultrasonic wave is emitted by the transmitter at a specific angle to the drum's tangential line to create a Lamb wave in the drum's shell. This Lamb wave then travels around the drum circumference creating longitudinal waves along its path which can be used to detect the time of flight of the Lamb wave around the drum. The pattern of and angle of the Lamb waves detected provides indications of defects and validates the measurements.

5.2 Description of the method

5.2.1 Objectives

The aim of this section is to assess the suitability of non-contact ultrasonic transduction in condition monitoring and inspecting (CM&I) of Magnox ILW 500 L drums. The system proposed will provide a non-contact tool to inspect the drums in-situ while they are stacked in their stillages via the small access gaps in the stillage structures. The system is expected to operate without any modification to the drums or their environment. The ultrasonic inspection data is expected to provide:

- discontinuity/crack screening
- encapsulation expansion monitoring
- warping and expansion detection
- container's internal pressure measurement
- internal and external corrosion cavity detection
- point thickness measurements
- potential detection of internal surface corrosion/erosion
- potential detection of liquids between the cementitious contents and stainless-steel walls

The ultrasonic inspection process is expected to be complimented by optical/laser scanners to identify the drum contours, align the ultrasonic transducers, and detect visual surface corrosion. The fusion of the ultrasonic and optical/laser scans will then be used to increase the chances of creating a true measured digital twin of the containers for long term monitoring.

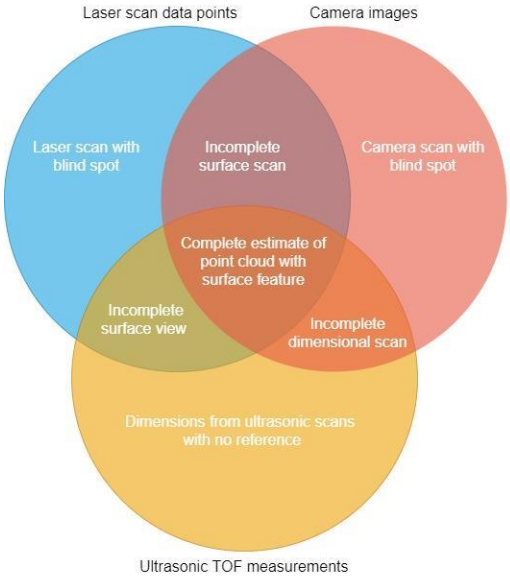

Fig. 20: Connection between inspection techniques used in this section.

5.2.2 Air-coupled ultrasonic inspection

The research started in academia as a project to use optical scanning for inspecting ILW drums in-situ, as the research progressed, it became clear that the optical/laser scanning is very limited due to the direct line of sight obstruction caused by the stillage structures and access restrictions.

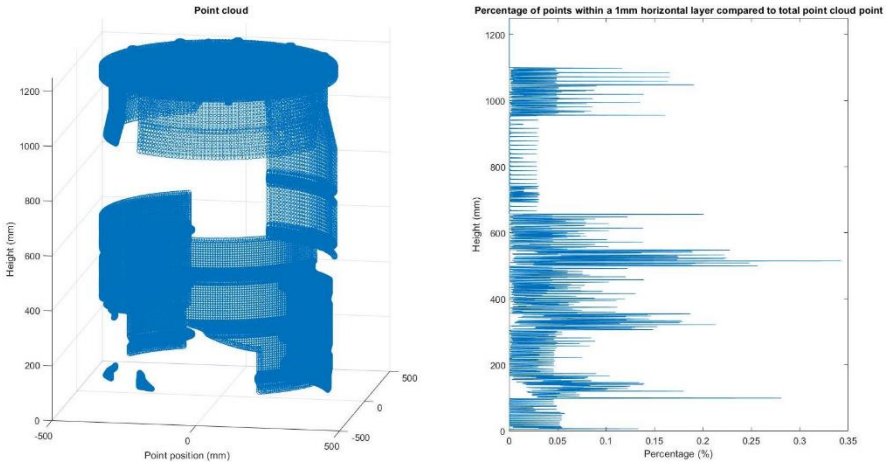

Fig. 1: (Left) Point cloud of an incomplete ILW 500 L drum from direct line of sight scan simulation. (Right) percentage of point present in 1.0 mm layer of the complete point cloud.

This directed the research to focus from optimising optical scanning to finding a new means of inspecting surfaces inaccessible via direct line of sight. Several technologies were considered at the time including high energy X-ray, muography and eddy currents, but ultrasonic inspection was chosen for the task due to its size because the project focus on in-situ inspection remained.

Several ultrasonic inspection techniques were considered and tested, most of the techniques were disregarded at the early stages of experimentation because they involved the use of coupling fluids and/or contact with the drum surfaces. Air-couple ultrasonic transduction however offered a non-contact, non-destructive and non-invasive mean of inspection at the cost of

- Transducer's alignment challenges

- Data validation complication
- Inspection access limitation

These costs were deemed acceptable because existing technologies are available to overcome them.

5.3 Test scenario and preliminary outcomes

Physical tests proofed feasibility of using non-contact air-couple ultrasonic transducers to measure the circumferential cross section of an ILW 500 L drum via a restricted access point. The system was able to measure the circumference of an empty drum with **2 mm** accuracy via a gap approximately 30cm in width.

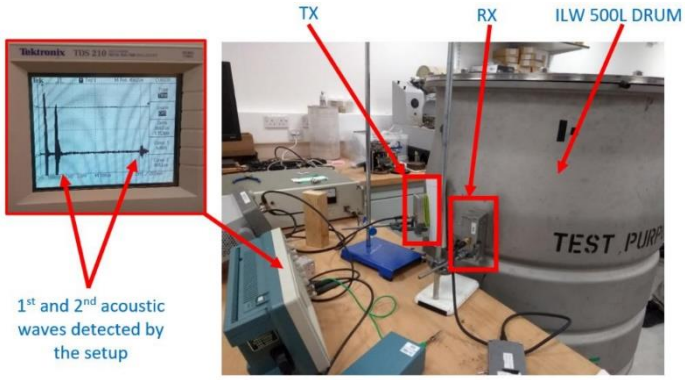

Fig. 2: Air couple transmitter (TX) and receiver (RX) setup generating and receiving a wave on/through the surface of an empty ILW 500 L drum sample and an oscilloscope view of the acoustic waves detected by the receiver during the successful wave generation/detection

Improved alignment technique and signal filtration was able to induce ultrasonic lamb waves and detect them travelling around an empty ILW drum more than 8 times. This provided a better platform for defect detection and measurement validation using detection pattern algorithms.

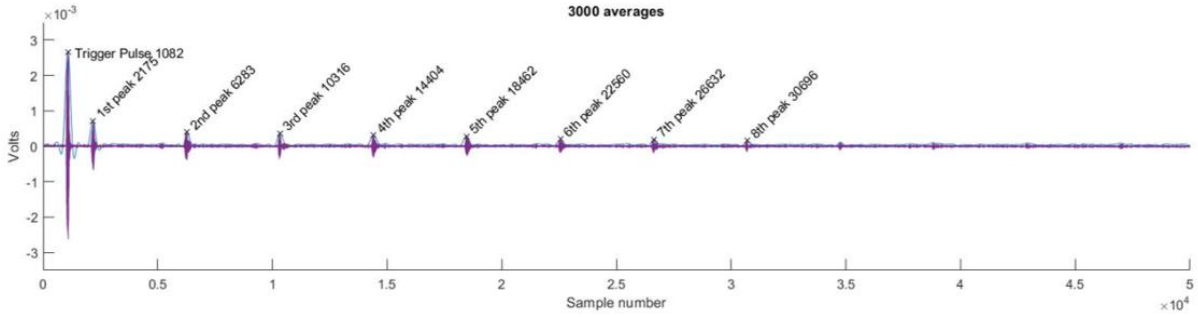

Fig. 3: Detection of the Lamb wave for the 8th time using signal filtering and averaging.

The ultrasonic transducers were also able to detect hairline cracks in samples manufactured using the same material and dimensions as that of the ILW drums. The discontinuity/defect position were irrelevant to the transducer position. In other words, the transducers can be placed in any location along the drum circumference and will still be able to detect and locate the discontinuity/crack due to the circularity of the drums, and the fact that the ultrasonic lamb waves are able to bypass the crack and travel around the circumference multiple time to detect it from different directions and positions.

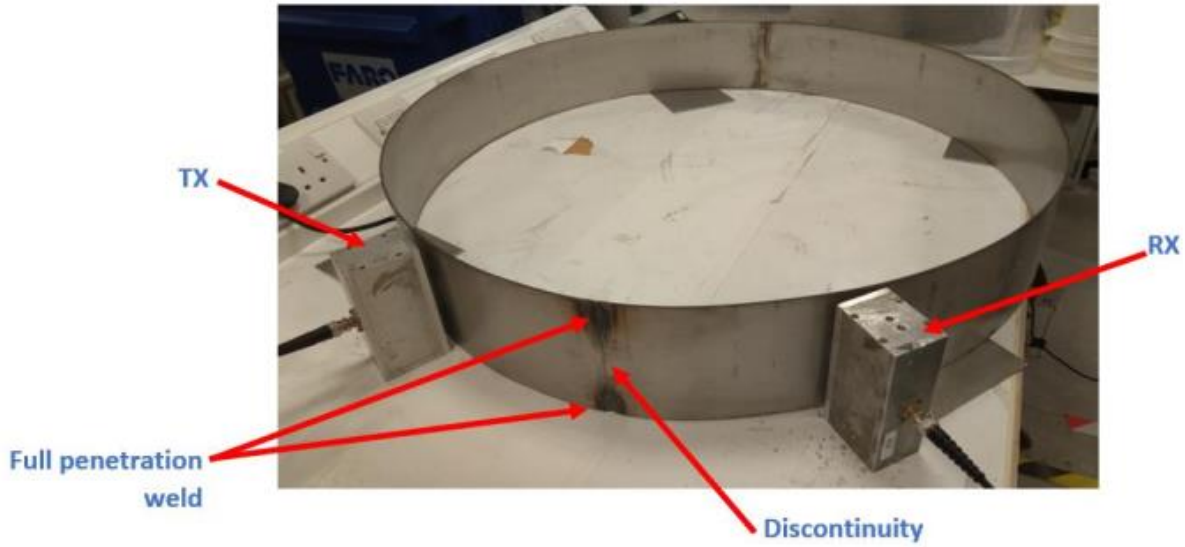

Fig. 4: Defected 800m diameter 316L stainless-steel sample being inspected using a pair of air-coupled ultrasonic transducers

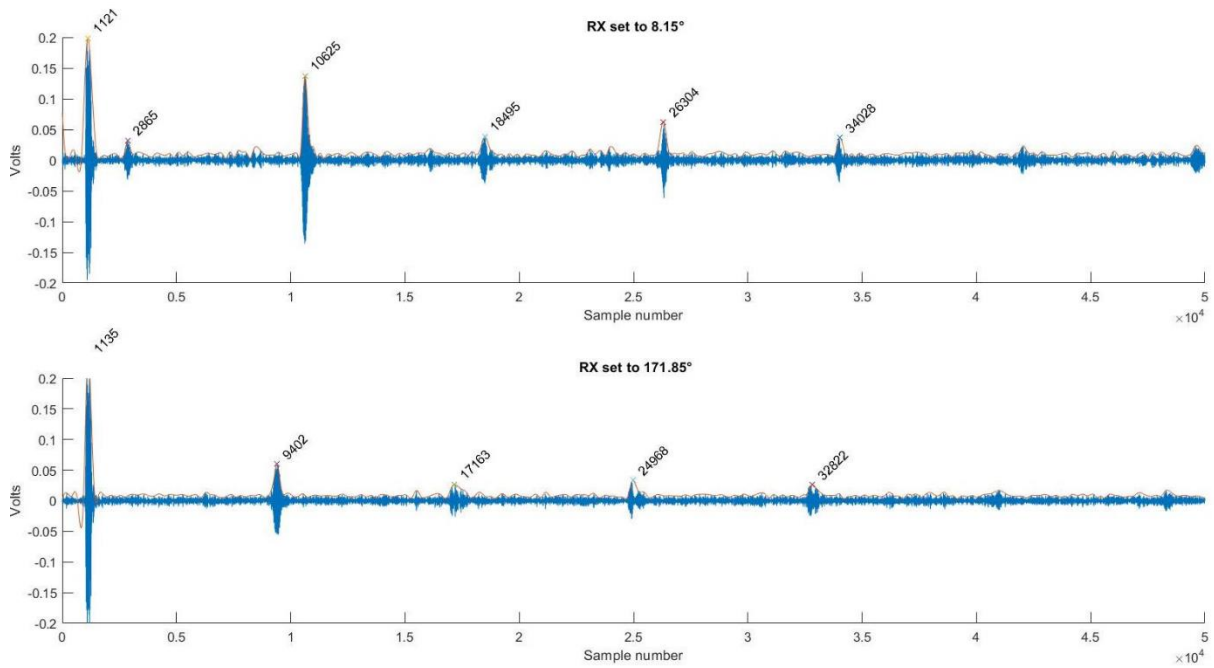

Fig. 5: (Top) Lamb wave detections with the transducer RX pointing towards the TX at 8.15 ° for circumferential measurement. (Bottom) Detection of Lamb waves reflected by the defects using the RX at 171.15 °

Another experiment was performed to identify the effects of the cementitious contents of the ILW drums on the ultrasonic lamb wave propagation.

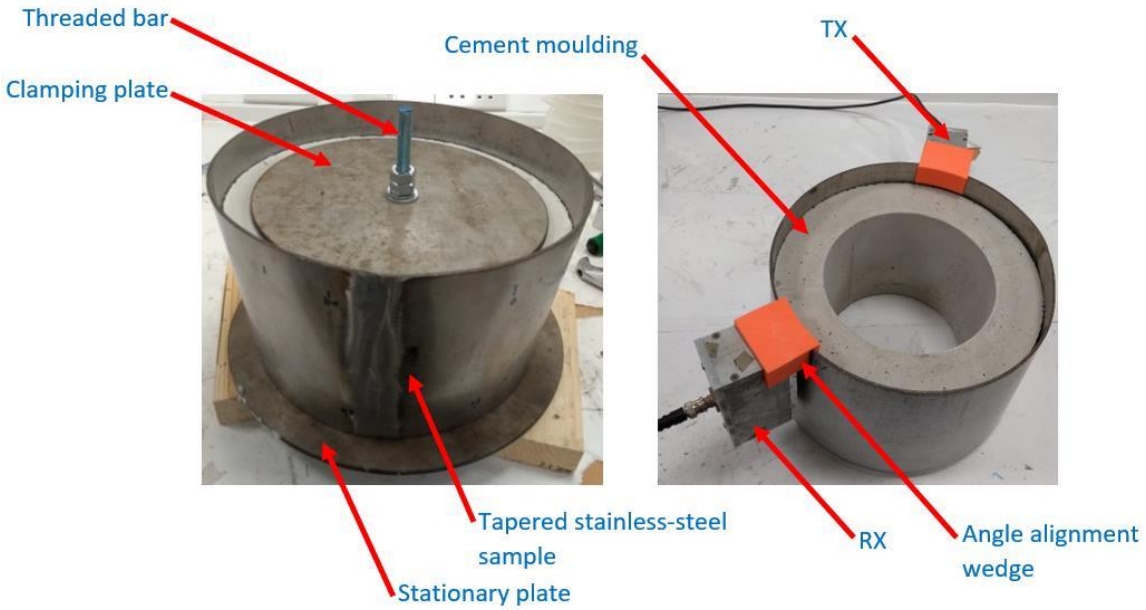

Fig. 6: (Left) Cement moulding being pressed into the Stainless-steel tapered sample using an M12 threaded bar. (Right) TX and RX mounted onto the tapered sample for circumferential measurements.

The results indicated that the increase in the internal pressure of the sample caused by cementitious content expansion causes a dampening effect on the lamb waves, which causes a drop in amplitude of the wave detected. This can potentially be used to measure the pressure build-up inside the drum using the same signal that is used to measure the circumference and detect defects.

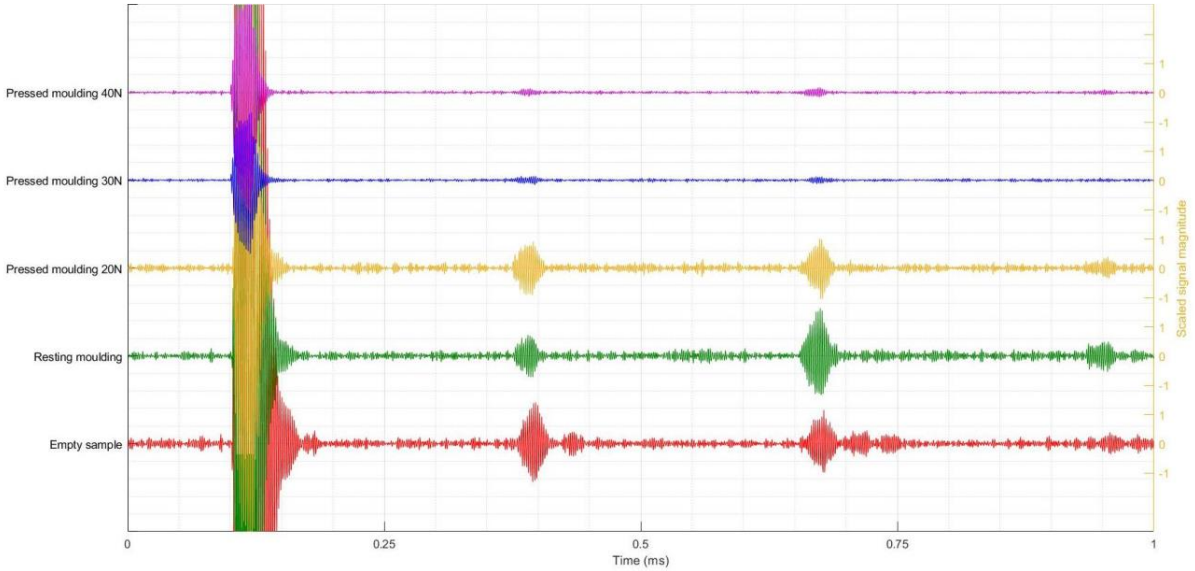

Fig. 7: Results compilation showing the amplitude drop in the lamb waves caused by pressure build-up inside the sample. (Note: The forces on the graph are the torque measurements of the clamping fasteners, not the true pressure inside the sample)

The non-contact air-coupled ultrasonic transduction system proofed that the technology could measure the circumference and detect discontinuity/crack as well as pressure build up inside the ILW drums with restricted minimal access to the drums.
The circumferential measurements were performed on real full scale empty drum samples.

Experiments were completed using the same setup to detect pressure build up using stainless steel samples with a matching material thickness and properties, and mechanical pressure build up using tapered cement inserts with composition matching the Magnox embolization cement mixture. Currently this qualifies the system to screen for abnormal pressure build up in the ILW drums.

5.4 Optical scanning validation study

To validate the point cloud simulation results presented in Figure:1, and identify the automated optical scanning process limitations, a KUKA robot was used to deploy a 3D Phoxi laser scanner to inspect deformed ILW 500L Magnox drums while they are stored inside stillages. The test was performed using a mock stillage and real aged and deformed Magnox drums. The robot was programmed to manoeuvre the Phoxi camera around the stillage to scan one of the drums inside the mock stillage, to confirm the access limitations and blind spots identified by the simulations.

Fig. 8: A KUKA robot deploying a 3D Phoxi laser scanner to inspect a deformed ILW 500L Magnox drum while stored inside mock stillages at the NNL facility.

The test revealed that aside from the access challenge caused by the stillage structure blocking the direct line of sight of the optical sensor to the drums, the minimum distance between the sensor and the drum required for the scanner to operate exceeds the expected gap between the stillage stacks. This means that for an optical 3D scanning system to successfully scan ILW drums in-situ while they are stored in stillage stacks, they shall be able to operate within a few millimetres away from their target. This will reduce the scanning area significantly, forcing the scanner to acquire more images to be able to cover the surface of interest, leading to longer scanning durations and more reliance on the robot's manoeuvrability to cover all the locations of interest.

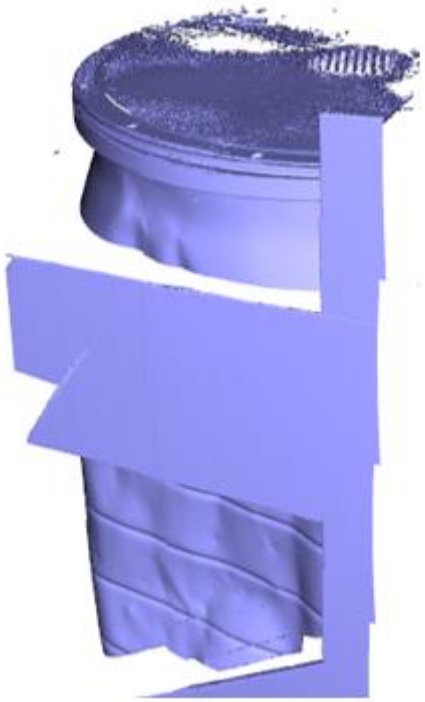

Fig. 9: 3D point cloud scan of the ILW 500L Magnox drum scanned using the Phoxi camera deployed by the KUKA robot in Figure 8

The severity of deformation on the surfaces with direct line of sight access can potentially be quantified using off the shelf software such as “GOM” that compare 3D point clouds to CAD models.

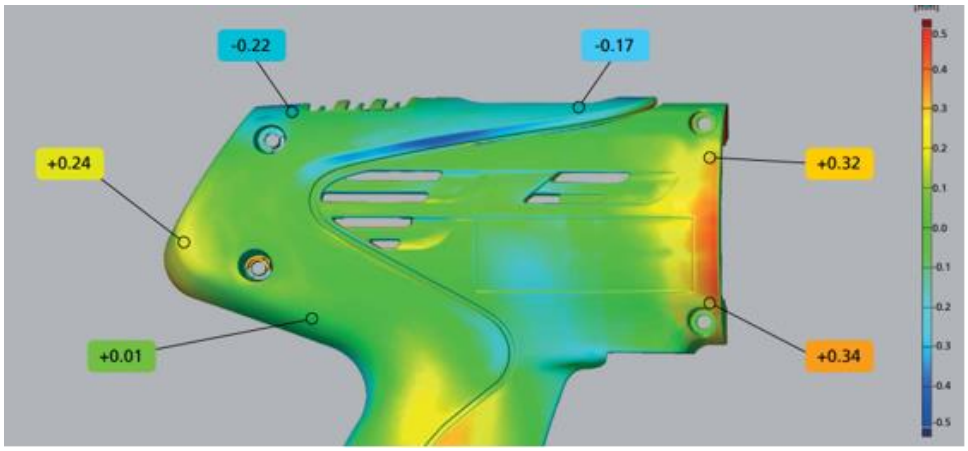

Fig. 10: Illustration of how off the shelf software can be used to quantify discrepancies between CAD models and 3D point cloud scans.

On the other hand, the deformations in the surfaces beyond direct line of sight will require the ultrasonic inspection methods described in the previous section.

5.5 Summary and Outlook

- Validate the ultrasonic circumferential measurements using real full scale filled/encapsulated drum samples.
- Induce defects into real full scale filled/encapsulated drum samples to validate the discontinuity/defect detection process.
- Calibrate the system to promote the pressure build up screening process into a pressure measuring process.

- Automate the ultrasonic transducer locating and alignment process to speed and improve the transduction process.
- Fuse the ultrasonic readings with real-life point cloud scan to create a true measured digital twin of full scale real ILW drums.

6 Muon Tomography

P. Andreetto, P. Checchia, E. Conti, F.Gonella - INFN Padua Unit
M. Romoli - INFN Naples Unit
P. Finocchiaro - INFN LNS Unit
C. Sabbarese, A. D'Onofrio - UNICAMPANIA (LTP)

6.1 Background

The Muon Tomography technique (Mu-Tom) is an interesting and promising way to investigate the internal unknown composition of cemented drums in a non-destructive manner. An existing INFN demonstrator apparatus can contribute to evaluate the capabilities and limitations of such a technique. Some preliminary tests have already been performed with satisfactory results.

6.2 Description of the prototype/method

The muons produced by cosmic rays are highly penetrating particles that can cross large amount of matter without being absorbed. Their trajectories are affected by the interaction with the matter itself, in particular, by the Multiple Coulomb Scattering. The distribution of the diffusion angles depends on the density, the atomic number Z and the thickness of the materials. The scattering angle is therefore a probe to explore the inner content of radioactive waste drums, which avoids the risks of a more destructive intervention.

In the past years, the INFN Padua group developed a demonstrator apparatus for the Mu-Tom that can be used, in the framework of the PREDIS project, for such purpose (see fig.1). The system consists of two muon detectors (the Muon Barrel Drift Chambers of the CMS experiment at the LHC accelerator at CERN [1] placed at about 3m apart from each other. The useful volume for the inspection of materials is 2.5m x 1.8m x 1.1m, enough to accommodate a standard waste drum.

Preliminary tests of the Mu-Tom technique have been already performed using a cuboid mock-up (73 x 73 cm^2, h = 48 cm), built with commercial concrete bricks (10.5 x 21 cm^2, h = 8 cm) as described in [2] (see also fig.1).

6.3 Test scenario and preliminary outcomes

A cemented drum has been recently produced by the colleagues of the UJV Institute to simulate a real radioactive waste cemented drum. Such muck-up contains unknown (and non-radioactive) metallic bodies in different positions inside the concrete, with different elemental composition, dimensions, and shapes.

The mock-up has been delivered and installed in the INFN-Padova MU-tom demonstrator as shown in fig.2. We acquired data in runs of several days each (about 13 days in total), to get significant statistics. Interesting and promising results have been obtained: the mock-up is clearly visible with a simple "radiography" (2D projection) as well as the most relevant metallic objects as shown in fig.3.

The technique is capable to produce 3D images and to scan the object at different horizontal layers using the 3D reconstruction algorithm (although the apparatus is not optimized for the vertical coordinate). We can select a different range of vertical voxels (1.5 cm size) at a different height on the cylinder.

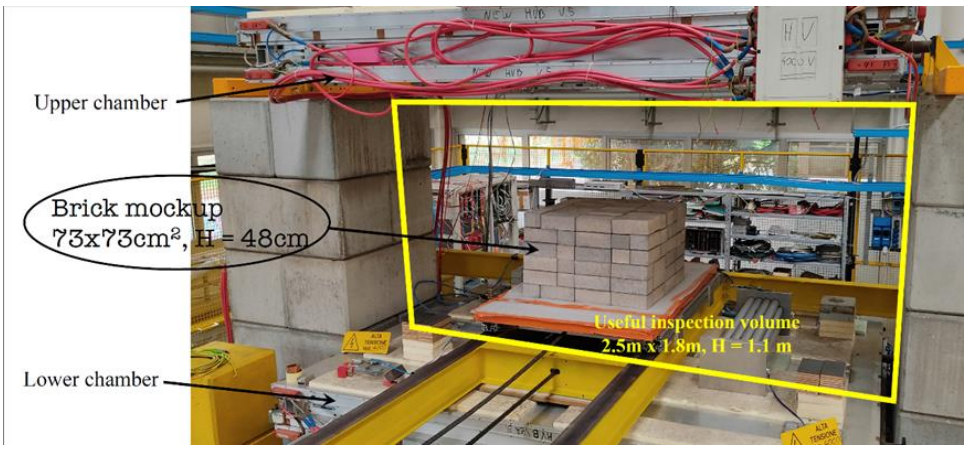

Fig. 1: A photo of the INFN Padova Mu-Tom demonstrator. The useful inspection volume, about 5m^3, is probably the largest in the world. A cuboid, 0.25m^3 volume, composed by cemented bricks, is also visible, used for the preliminary test.

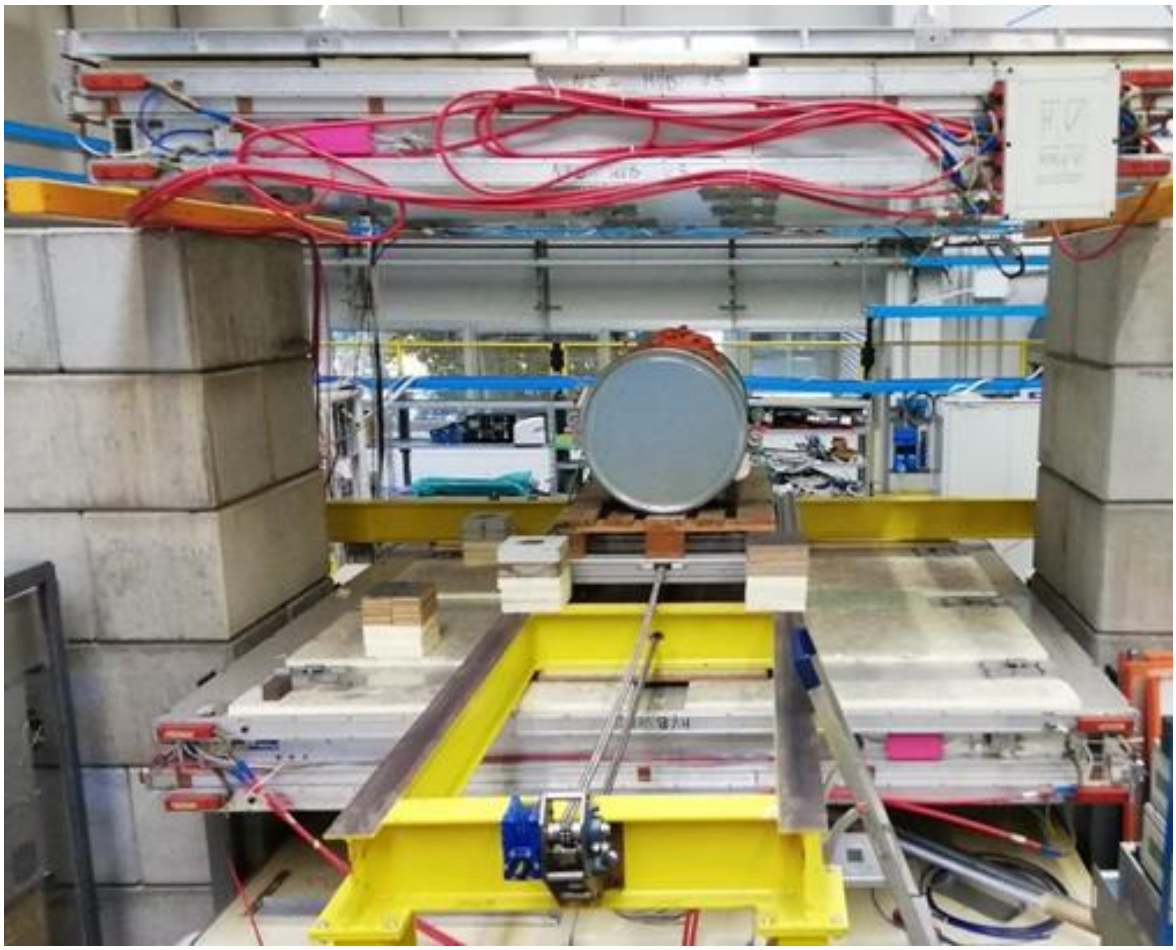

Fig. 2: A picture of the new mock-up produced by UJV installed in the INFN Padova Mu-Tom demonstrator.

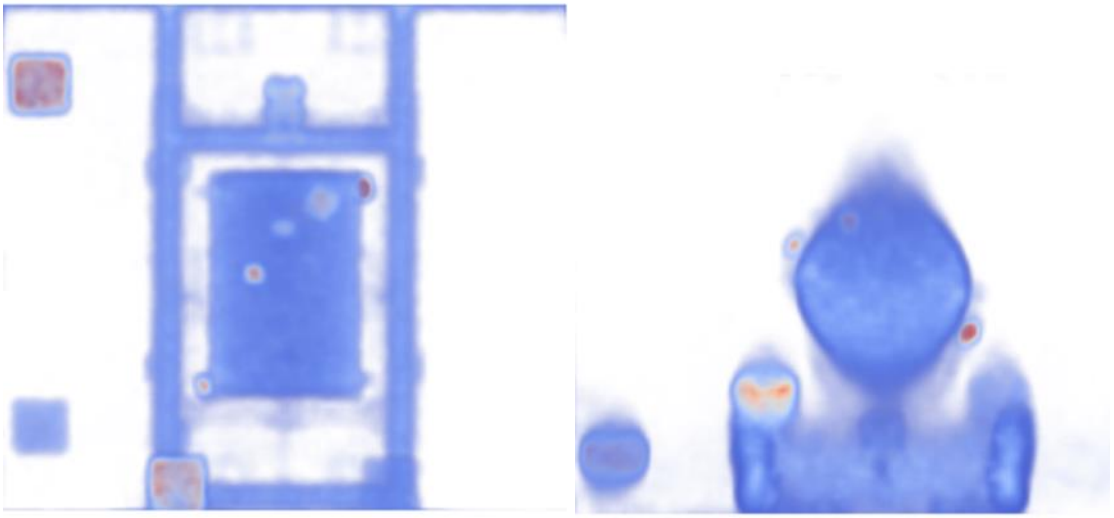

Fig. 3: Left: Top view 2 D reconstruction of the demonstrator inner volume. Right: Front view. The drum shape is clearly visible with some objects inside. Note the presence of several external objects acting as support structure or reference calibration.

As an example, Fig. 4 shows the image obtained selecting only four horizontal layers of voxels, equivalent to a 6 cm thickness, in the lower part of the drum. Two objects, not visible in fig. 3, are clearly appearing.

The experimental apparatus detects only vertical muons, providing a good image reconstruction in the horizontal plane. The vertical coordinate is measured with a much lower resolution, which lead to blurred images, as seen in the in Front view reconstructions of Fig.3. Since we cannot to rotate the muon detectors to collect horizontal muons, we can get around the problem by rotating instead the object under inspection by 90 degrees, provided that a precise reference frame is established and measured to control the rotation. Additional lab tests and software algorithms are then required to optimise the mock-up reconstruction.

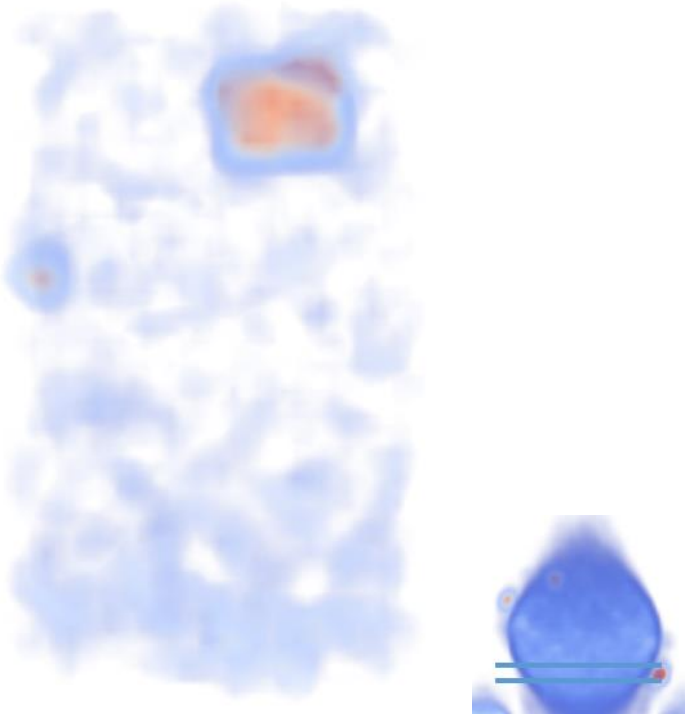

Fig. 4: Left: Top view image of a limited range of vertical voxels. Right: front view image with two green lines indicating the considered vertical range.

6.3 Additional Lab tests

To develop an effective system for evaluating the roto-translation of the mock-up drum, we have installed four spheres made by Tungsten, 5 cm diameter. They are positioned at a reasonable distance from the cylinder body so that their positions in space can be measured with precision (fig. 5) without interfering with the image of the drum itself.
We will gather a significant amount of data using cosmic muons in at least three mock-up positions: one with the vertical drum (as shown in fig. 5), and at least two with the horizontal cylinder rotated approximately 90 degrees around its axis. The analysis of such a big dataset will follow.

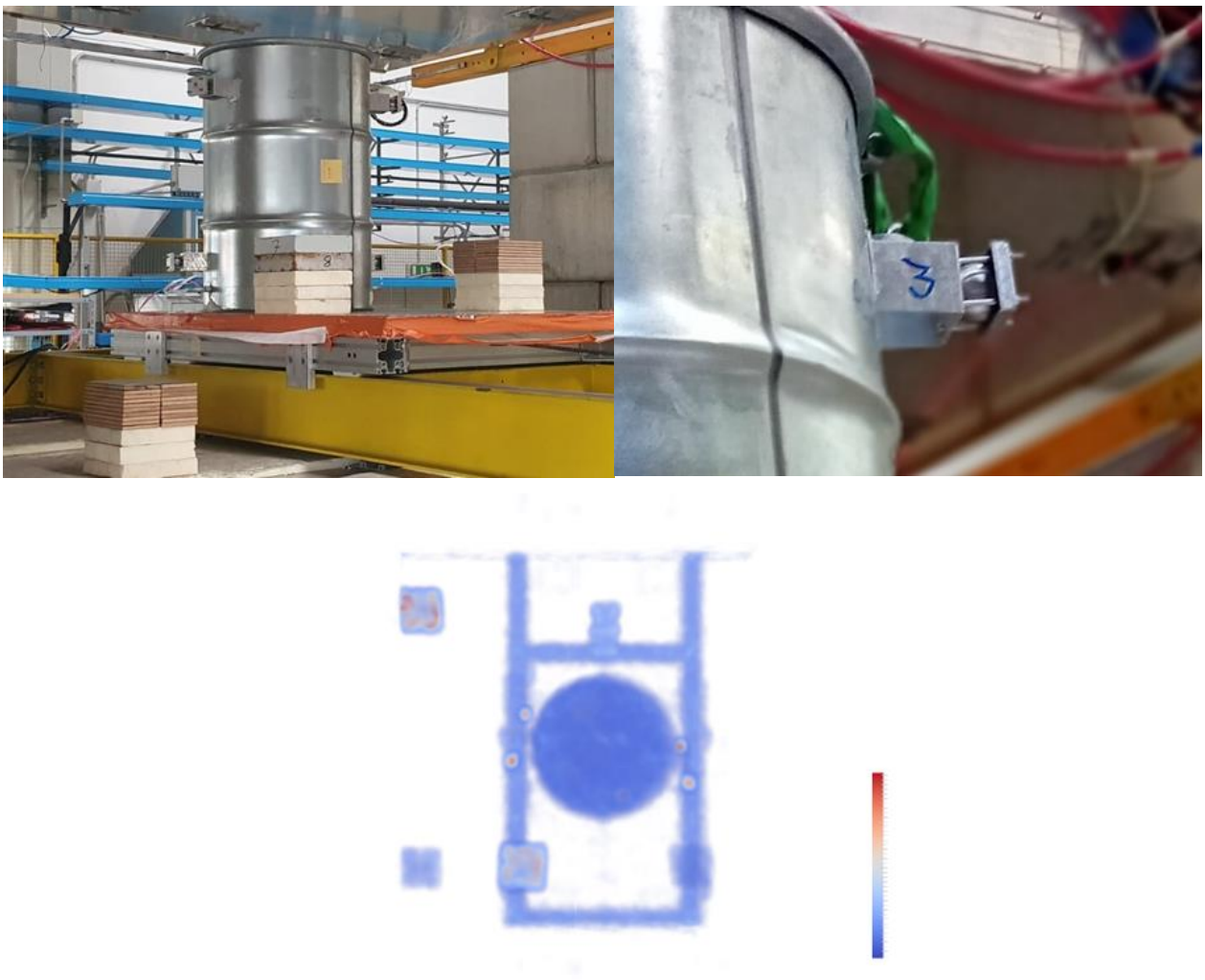

Fig. 5: Upper Left: The new mock-up with the reference W balls. Upper Right: detail of a W ball mounted on the drum side. Lower: top view reconstructed image with the four W balls clearly visible on the side of the cylinder.

6.4 Summary and outlook

After the study of two different mock-ups in the Padova muon tomography system, we have demonstrated that Muon Tomography is capable to detect metallic objects embedded in large concrete blocks. To quantify the ultimate performance of this technology, more data are going to be taken and analyzed.

6.5 References

[1] The CMS collaboration, S. Chatrchyan et al., JINST 3 S08004, 2008.
[2] Checchia, P. et al.: “Muon Tomography” contribution to PREDIS Predis_WP7_MilestoneM7-5_MS53

7 Embedded SensorNet: characteristics, lab environment, and preliminary test

Leone Pasquato, Christoph Strangfeld, Ernst Niederleithinger
Bundesanstalt für Materialforschung und -prüfung (BAM), 12205 Berlin, Germany

7.1 Background

BAM (Federal Institute for Materials Research and Testing) is developing an electronic measurement system to be placed inside a waste drum, which will be filled with concrete. The goal of this measurement system is to monitor the process of hardening and the evolution of the concrete itself over time to indirectly identify potential defects such as corrosion or cracking. The measured parameters are humidity, temperature, and pressure. In this regard, particular attention was given to the design of the electronic board's enclosure, to allow the sensors to measure the state of the concrete without being in direct contact with it. In the scope of the European Commission's project of PREDIS, the supply of power to the battery-less sensors and the data acquired by such sensors are transmitted through the metallic waste drum by an innovative wireless technology developed by VTT (Technical Research Centre of Finland) to ensure long-term operation while keeping the integrity of the sealed container.
The sensing system is made of a chain of small units, called SensorNodes. Each SensorNode includes two off-the-shelf sensors, with one for relative humidity and temperature and one for pressure and temperature. A SensorNode is designed to have a unique identifier, to be connected to other units while being uniquely discoverable by a standard communication protocol. In this way, a distributed matrix of measurement points is created.
One of the most challenging tasks in designing a measurement system to run in a harsh environment (such as hardening concrete) is to let the sensors sense the external environment without damaging the sensors themselves. To keep the external environment away from the electronic board while still letting the sensors measure the concrete behaviour, holes have been drilled through the lid and covered from the inside with a layer of porous membrane. The membrane's pores allow water and gas particles to pass through and let the enclosed air equilibrate with the external environment. With the help of the developed sensors, monitoring concrete in cemented waste drums will be possible. The derived data will also serve as the basis for ongoing modelling approaches for digital twins within the PREDIS project. Overall, the sensors provide a means of enabling safe nuclear waste management through advanced monitoring.

7.2 Description of the prototype/method

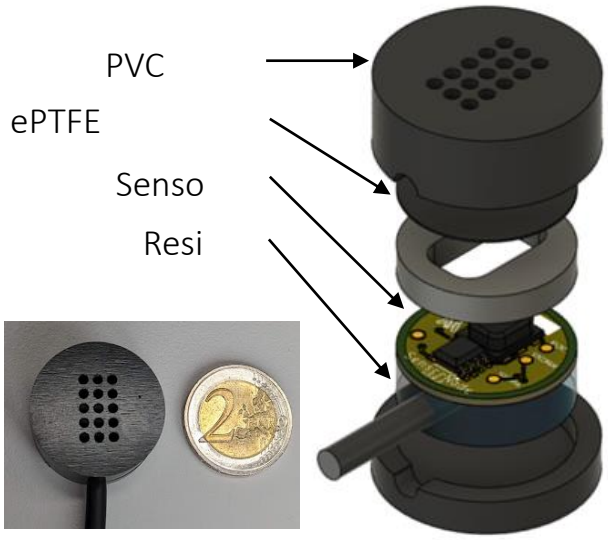

Fig. 6: SensorNode

One of the most challenging tasks in designing a measurement system to run in a harsh environment (such as a hardening concrete) is to let the sensors sense the external environment but without damage to the sensor itself. Since concrete is an alkaline solution, a particular attention on the choice of the materials and the sealing techniques must be done.

7.3 Test scenario and preliminary outcomes

The experiment has been carried out embedding the HoneyWell-based system and the ST's SmarTag board in concrete. Since the goal concern also the inspection of the sealing technique, the experiment has been repeated two times to evaluate the sealing technique through extraction of the sensor boards after the first run.

7.4 Technical Development

7.4.1 SensorNode Design

The SensorNode is a custom-made device designed to incorporate multiple off-the-shelf sensors within a single unit, offering the capability to connect multiple units through the same communication bus. A tailored enclosure is needed to use the SensorNode in harsh environments, such as hardening concrete, to protect the electronic board while letting the sensors measure the external environment. This objective is achieved through the strategic implementation of a porous membrane, effectively shielding the electronic board from external forces. The membrane's permeable pores facilitate the passage of water vapor and gas particles, allowing the enclosed air to equilibrate with the external environment. Consequently, the sensors can precisely measure the state of the confined air volume isolated by the membrane and the casing.
One measurement cycle for each node requires about 0.4mAs (20mW x 60ms).
Onboard sensors:

- Absolute Pressure (0 to 400kPa)
- Relative Humidity (0%RH to 100%RH)

- Temperature (-40 °C to 125 °C)

Limitations:

- Max 64 nodes on the same bus (Unique ID limit)
- Max 6m water depth (Membrane's permeability limit)
- Max 10m cable length (Communication protocol limit)

7.4.2 Data storage

A device called Network Gateway, based on a RaspberryPi board, has been integrated in the data acquisition system. It is responsible to store the measurement data on a physical USB stick and upload them on an InfluxDB instance hosted on the Azure platform.

Following the InfluxDB best practices, data are organized in two measurements: Energy and SensorNet.

- Energy is the voltage of the capacitor (in the Embedded Unit) at the end of the measurement routine.
- SensorNet contains the data from the SensorNodes.

Each measurement has some fields, that represent the actual measured values. Tags are added to the fields in order to filter and address the data (e.g., all the temperature values of the SensorNode 1)

Measurement	Field (double)	Tags (string)
Energy	voltage	drum_id
SensorNet	temperature	drum_id, sensornode_id, status
SensorNet	humidity	drum_id, sensornode_id, status
SensorNet	pressure	drum_id, sensornode_id, status

Fig.7a. Data structure in InfluxDB

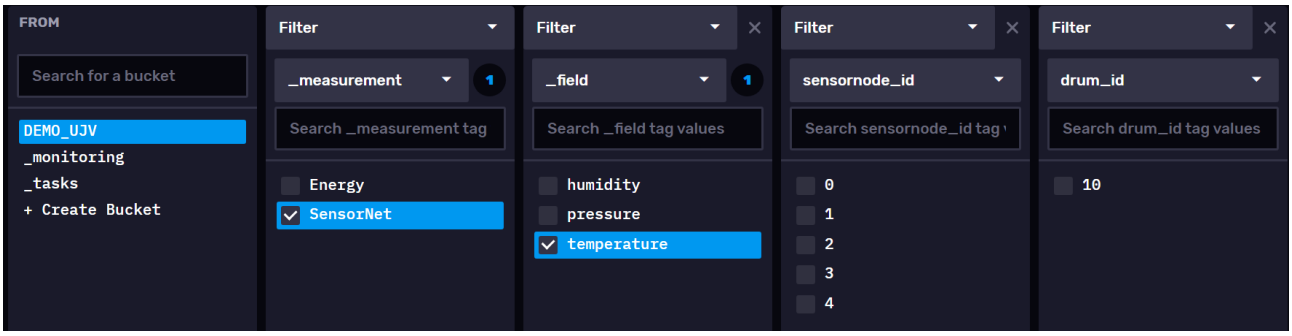

Fig.7b. InfluxDB Data Explorer View

7.5 Lab Test

To test the optimized design, an experiment with a 40cm height pipe has been setup. One SensorNode has been embedded in the pipe and one is kept outside to have a reference with the external environment. After 5 weeks the sensors are still operative.

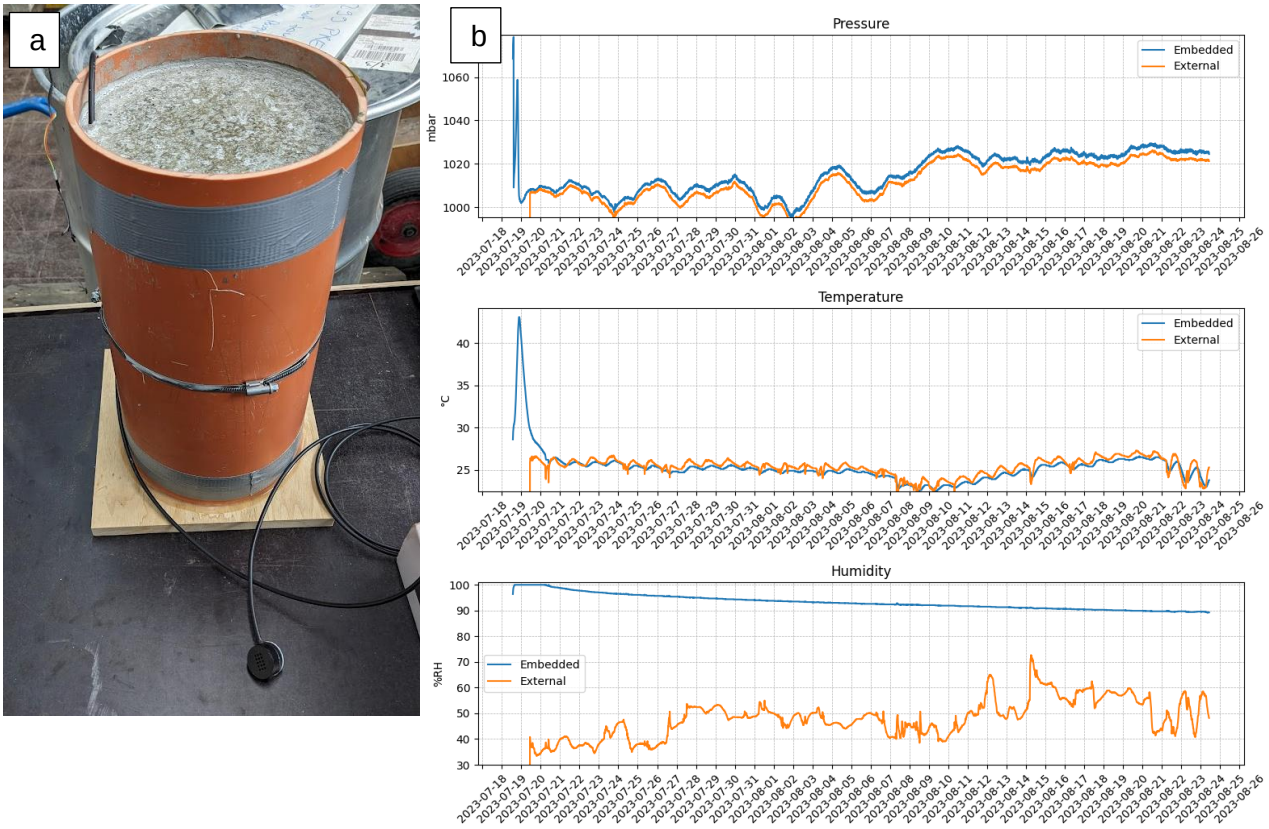

Fig. 8: a) Specimen b) 5 weeks of data

A real-scale experiment is going to be set up. Five SensorNodes have been installed in the inner surface of a steel drum, while the main components of the VTT's RFID system (RFID transmitter and receiver). Data transmission has been tested successfully from the sensors through the metal plate.

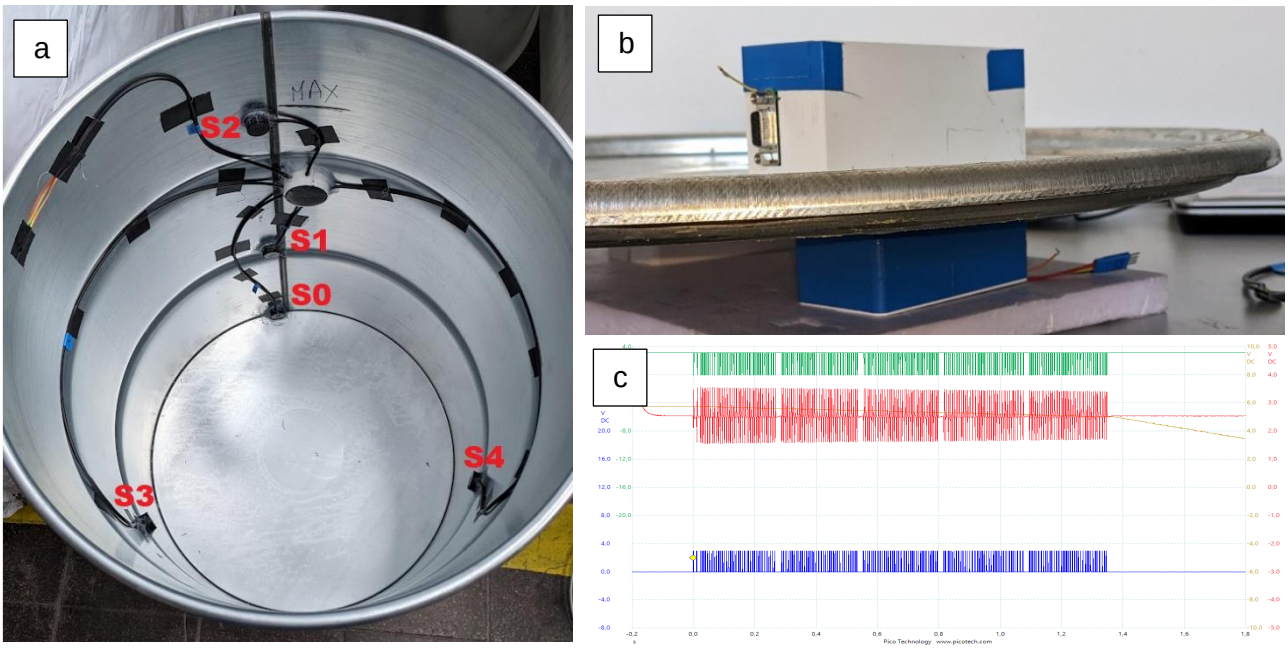

Fig.9: a) Layout of 5 SensorNodes in the drum. b) VTT's RFID receiver and transmitter mounted on the drum's lid. c) blue: Embedded RFID transmitted data, red: External RFID received data, green: decoded data in the External microcontroller Unit

7.6 Test in Realistic Environment

The drum equipped with the instrumentation has been filled with Portland cement CEM I 42,5 N and then sealed with the instrumented lid. The embedded SensorNodes have been connected to the Embedded RFID unit by using a waterproof connector. After the concrete dried out, the drum has been transported to UJV for the preparation of the DEMO test.

Fig.10. Concreting and transport of the drum

In UJV, the drum has been placed in stillages among other mockups. The External RFID unit placed on the drum's lid has been connected by a 10m cable to the microcontroller unit and the network gateway placed in the nearby room. The microcontroller unit has been configured to perform one measurement every hour, the network gateway stored the data locally on a USB stick and upload them on InfluxDB, through an Ethernet connection.

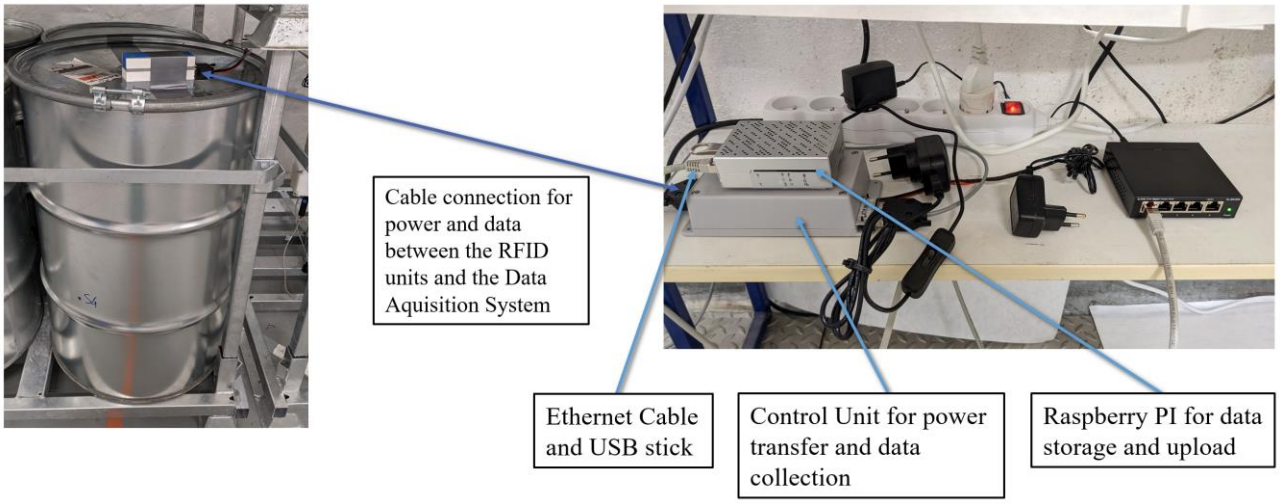

Fig.11. DEMO test setup

Data have been collected for three months, with sporadic missing uploads. The measurements from the SensorNode1 are likely not reliable since the temperature is saturated to the maximum value and the pressure has an offset with respect to the others. The humidity measures are stuck to 100%, performing measurements in the next months will give more information to explain this behaviour. The voltage of the interim storage in the Embedded RFID unit is stable around the default value, that means the communication through the metal lid remained stable, that means the Embedded unit remained well fixed to the lid and the distance with the External Unit didn't increase.

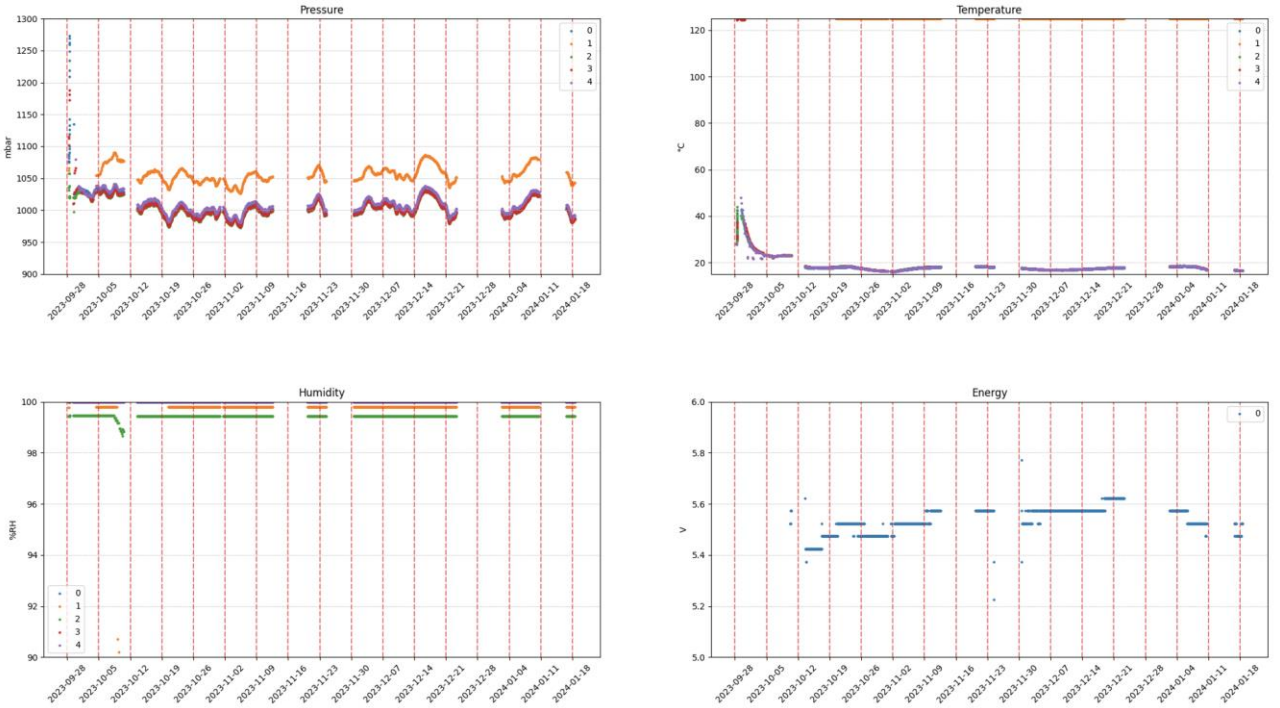

Figure 21. Measurement data

7.7 Summary and Outlook

The feasibility of embedded concrete monitoring using a custom device has been demonstrated. A small-scale test has illustrated that the sealing technique effectively prevents damage to electronic circuits during concrete hydration. However, additional experiments are required to assess the long-term resistance of the materials used and the reliability of the measurements.
There is room for improvement in the design of the SensorNode. The major issue has been faced in the early stage of the monitoring when the concrete was still fresh. The moisture absorbed by the dielectric insulator of the cable used to connect the SensorNodes increased the capacitance of the communication bus. That leads of an increase of the rising times of the pulses and the inability of the communication protocol to decode them. This can be fixed by using lower moisture absorption cables with a lower capacitance. There is also potential to optimize the time response of the system by refining the shape of the enclosure. This includes reducing the volume around the sensors, thereby decreasing the time required for the internal air volume to equilibrate with the external environment. These enhancements could contribute to the overall effectiveness and versatility of the monitoring system.

7.8 References

Johann, S. e. (2017). RFID sensor systems embedded in concrete–Validation experiments for long-term monitoring. *The e-journal of nondestructive testing & ultrasonics*, Artikel-8.

Phung, Q. T., Frederickx, L., Nguyen, T. N., Seetharam, S., Laloy, E., Verbeeck, J., . . . Valgaeren, C. (2021). An integrated approach to assess the alkali silica reaction of cemented wastes . *Predis Workshop 2021*, (pp. 94-106).

Strangfeld, C., Johann, S., & Bartholomai, M. (n.d.). Smart RFID Sensors Embedded in Building Structures for Early Damage Detection and Long-Term Monitoring.

8 Wireless data acquisition from embedded battery-less sensors in waste drums

Esko Strömmer, Marko Korkalainen, VTT

8.1 Background

The scope of the work by VTT (VTT Technical Research Centre of Finland Ltd) has been enabling long-term operation and data readout of sensors embedded inside waste drums. A crucial technical constraint has been preserving the integrity of the steel drums by prohibiting any perforations through the steel cover, which might have been necessary if the embedded sensors had been connected by a cable. Moreover, the requirement for long-term operation has called for an alternative powering method of the embedded sensors without exhausting batteries. Thus, a wireless interface through the steel cover, taking care of both powering and data readout of the sensors, was considered necessary. For a more comprehensive demonstration of embedded monitoring in waste drums, another requirement has been the compatibility of the data acquisition system with the temperature, humidity, and pressure sensor of BAM (SensorNode), reported in chapter 7.

For powering and data readout of battery-less low-power sensors, there are existing short-range RFID technologies such as ISO/IEC 14443-1 (2018) or ISO/IEC 15693-1 (2018), but these cannot operate through solid metal layers. Thus, a specific inductive RFID-like wireless technology, capable of operating through the 1.5 mm thick ferromagnetic steel cover of the drum, was considered necessary for the embedded sensors in the waste drums. The goal of the work has been to develop a new wireless technology for this. Another goal has been to network the developed wireless technology through the steel cover further to a backend server.

Waste drums and other low-level and intermediate-level waste stuff are often stored in bigger prismatic containers that are made of reinforced concrete and stacked inside bigger storage spaces. For this, another goal has been to investigate and demonstrate the applicability of the developed wireless technology in condition monitoring of the concrete containers in their storage space. This application can be facilitated by extending the wireless operation range remarkably, which in this operation environment is possible by replacing the radio technology of the wireless link, originally developed for the waste drums.

8.2 Method

8.2.1 Overall architecture

Figure 1 shows the target architecture of the data acquisition system for embedded sensors in the drum. The transponder unit inside the drum is compatible with the SensorNodes of BAM and can be connected to the SensorNodes S0 – S4 by cables that involve four wires, two for powering the SensorNodes and two for communication with the SensorNodes by I2C protocol. The transponder unit is connected wirelessly through the steel cover to an external reader unit that is powered and controlled by an external microcontroller unit via a cable connection. For the handling and visualization of the SensorNode data, the microcontroller unit is connected to Influx data base via a Network gateway, the technical implementation of which is Raspberry PI single-board computer with custom software. The microcontroller

unit and the Network gateway are powered by off-the-shelf wall mount power supplies. There is also a local graphical user interface (GUI) running in a laptop computer, connected to the microcontroller unit by Bluetooth, for the installation and testing the sensor instrumentation on the spot.

A specific requirement in the development of the data acquisition system has been powering and reading the sensors from the outer side of the waste drum while keeping the integrity of the steel cover of the drum, which had been impossible if the embedded sensors had been connected to the outer side of the drum by a cable. Existing standard RFID technologies such as [1] or [2], as well as standard radio technologies in general, cannot operate through a solid metal layer, which in this case is 1.5 mm thick ferromagnetic steel. Thus, a specific inductive RFID-like wireless technology, capable of operating through the steel cover of the drum, has been developed in project PREDIS. The key components of the developed wireless technology are the battery-less transponder unit on the inner side of the drum, the reader unit on the outer side of the drum, and the microcontroller unit.

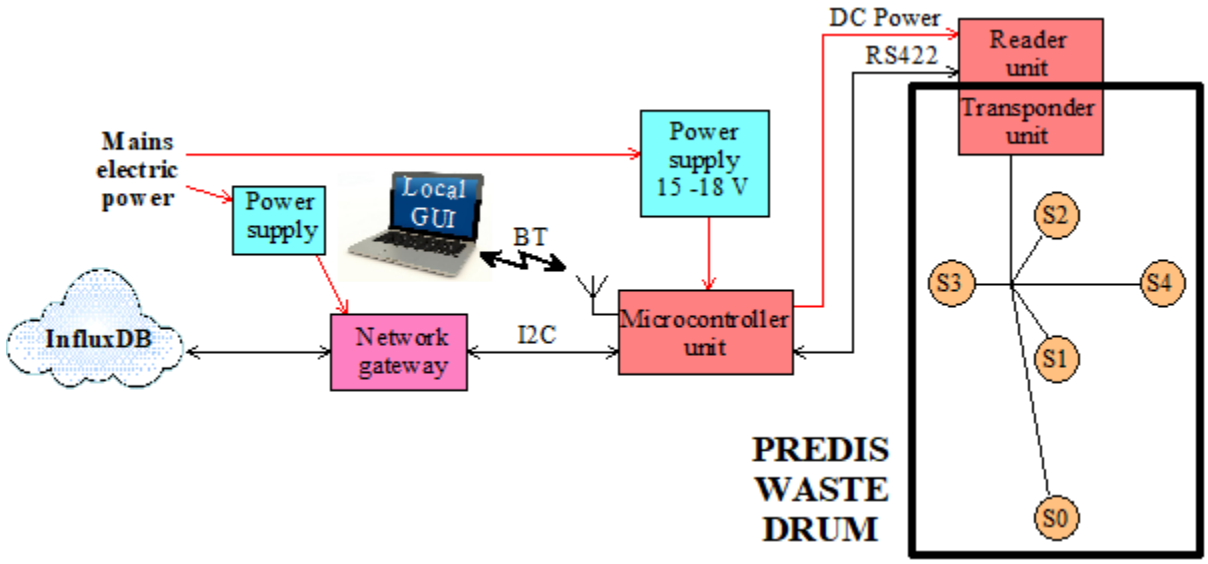

Fig. 1: Target architecture of the PREDIS data acquisition system for embedded sensors in the drum.

Wireless power transfer through metal layers by inductive coupling has earlier been reported in some research papers such as [3] and [4]. These papers deal with the optimization of the power transfer through non-magnetic metals without any data transfer. The wireless link developed and demonstrated in project PREDIS features both power and data transfer and can also operate through ferromagnetic steel. The technical implementation of the wireless link through the steel cover is discussed closer in the next chapters.

8.3 Technical development

8.3.1 Hardware of the wireless link through the steel cover

In addition to the electrical conductivity, the high magnetic permeability of the steel cover of the drum lowers the penetration of radio signals remarkably. To overcome this, the developed wireless technology deviates from the standard RFID systems in several ways:

- super-low frequency (SLF) radio band,

- ferrite core antennas,
- no resonance tuning of the antennas,
- active uplink data transmitter,
- data uplink modulation by short pulses,
- time-division multiplexing of the energy download and the data uplink.

To minimize the damping effect of the steel, the frequency of the carrier for energy download to the batteryless transponder unit has been reduced to 100 Hz. The attenuation of this frequency in ferromagnetic steel is much lower than the 13.56 MHz radio signal of the standard RFID systems. The carrier is generated in the reader unit by a class-D push-pull amplifier.
To enhance the inductive coupling between the antennas in the reader unit and in the transponder unit, and to facilitate proper impedance matching of the antennas, both antennas are based on a UR-type ferrite core (Ferroxcube UR64/40/20-3C90). For the encapsulation and mounting the transponder unit and the reader unit, the antenna coupler was designed to allow for a small gap (maximum 1 mm) at both sides between the steel cover and the ferrite cores. This was achieved by wiring the transponder unit antenna by 1600 turns of 0.21 mm enamelled copper wire, and the reader unit antenna by 250 turns of 0.34 mm enamelled copper wire.
In general, resonance tuning of the antennas improves energy transfer efficiency remarkably in inductive systems. However, in this case, resonance tuning is not applied to either of the antennas, since it would make the system very sensitive to the antenna displacements, which affect the antenna inductances considerably. Furthermore, resonance tuning would also slow down the data uplink speed. Even though the energy download efficiency without resonance tuning is much lower, it is sufficient to power the transponder unit with various connected low-power sensors.
To enable data uplink from the transponder unit to the external reader unit with low antenna coupling because of the attenuation of the steel cover, the transponder unit involves an active data transmitter instead of a load modulation circuit of the standard RFID transponders. To enable relevant bit rates with low antenna bandwidth, no carrier modulation is applied in the data uplink. Instead, the data symbols are comprised of 1 ms pulses, and the sensor data is encoded to the time interval between single pulses.
The active data transmitter also calls for time division multiplexing between the energy download and the data uplink. Each operation cycle starts by downloading energy into an interim energy storage in the transponder unit, which is able to detect when the charging process is completed and start the data uplink.
The operation of the wireless link through the steel cover is controlled by an nRF51422 microcontrollers of Nordic Semiconductor both in the transponder unit and in the microcontroller unit. The software of the transponder unit and the optimization of its energy consumption is discussed in the next chapter.

8.3.2 Software of the Transponder unit

The operation of the transponder unit is constrained by the limited availability of the supply power from its interim energy storage. This has also to be considered in its software design. The flow chart of the transponder unit software is shown in Figure 2.

In every SensorNode readout cycle, the software starts the operation after the energy reception circuit has switched on the nRF51422 microcontroller, which takes place when the interim energy storage voltage reaches 6.3 V. To minimize the microcontroller start-up time and thus also the start-up energy, the clock signal of the microcontroller is generated by its internal RC oscillator. The initialization of the microcontroller internal Bluetooth LE stack is kept minimal since it is not needed in the transponder unit. After the initialization of the microcontroller, the software reads a resistor-programmed drum ID and the sensors via the I2C bus. The energy reception can continue during this, which enables smaller size of the interim energy storage and thus also faster charging and lower residual energy in it. The software also switches on the internal DC/DC buck converter of the microcontroller to minimize the current sink from the interim energy storage.
After reading the sensors, the software starts to wait for the end of the energy download, during which it also keeps the interim energy storage voltage below 8.0 V by discharging possible excess energy through resistors. When the software has detected the end of the energy download, it waits for 2 seconds to allow the stabilization of the antenna circuits, after which it starts the sensor data uplink. The data from the sensors is encoded to successive data messages. Finally, the software discharges the residual energy from the interim energy storage, which also causes the energy reception circuit to switch off the microcontroller.

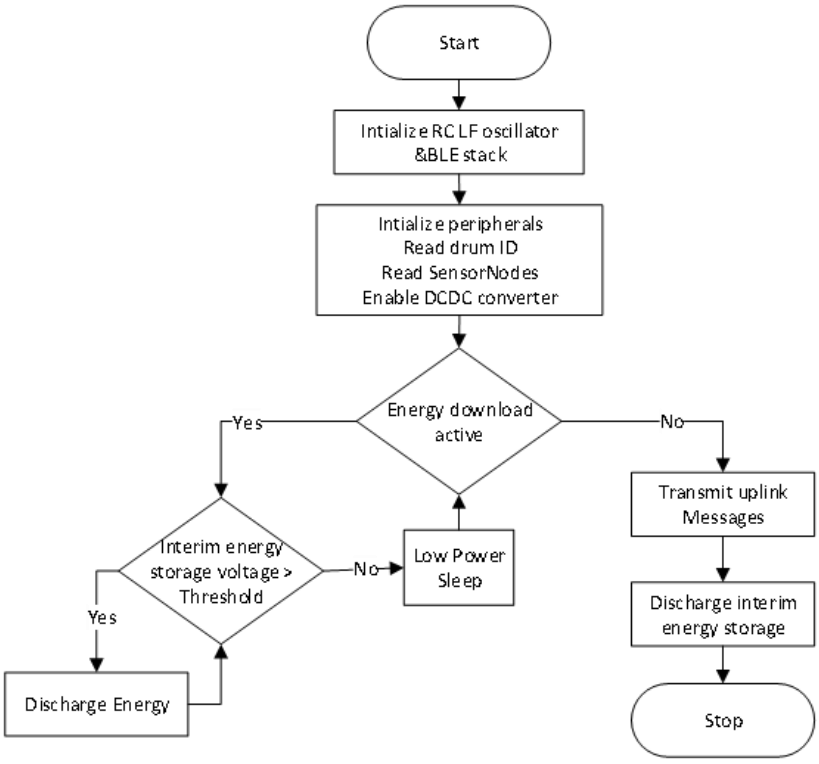

Fig. 2: Transponder unit software flow chart.

8.3.3 Software of the Microcontroller unit

Contrary to the software of the transponder unit inside the drum, the software of the external microcontroller unit is not constrained by the limited availability of supply power. Thus, the microcontroller can use its low-frequency crystal oscillator for generating its internal clock signal, and its Bluetooth LE stack to communicate with a laptop computer providing a local graphical user interface (GUI) for the sensors.

The carrier signal for the energy download to the transponder unit is generated by a timer that controls PWM generation. After the energy download, the microcontroller unit opens a listening window for uplink data reception. To avoid errors in measuring the intervals between data uplink pulses, a low jitter detection method is applied. Time intervals between the pulses are measured via a digital input by using high-resolution edge detection interrupts and events routed via PPI (peripheral to peripheral interconnect) interface to a timer peripheral capture. Detected bits are fed to a decoder algorithm, and successfully decoded messages passing a CRC check are transmitted to the local GUI by Bluetooth LE and to a Raspberry Pi based network gateway by I2C interface. Operation parameters such as the sensor sampling rate and the length of the energy download cycle can be changed by the GUI or via the network gateway.

8.3.4 Modification of the radio parts for monitoring concrete containers

Waste drums and other low intermediate level waste stuff are often stored in bigger prismatic containers that are made of reinforced concrete and stacked inside bigger storage spaces. The monitoring of concrete containers in their storage space can be facilitated by extending the wireless operation range remarkably, which in this operation environment is possible by different radio technology. The main modifications to enable applying the developed PREDIS wireless monitoring system to prismatic concrete containers with wireless operation range of several meters were the following:

- increasing the carrier frequency for energy download to 125 kHz,
- replacing the reader unit antenna by an air core antenna of size 2 m x 2 m and 4 turns,
- replacing the transponder unit antenna by a flat air core antenna of size 1 m x 0.6 m and 12 turns in spiral,
- applying resonance tuning of the antennas,
- replacing the short pulses by short 125 kHz carrier bursts in the data uplink modulation.

In the laboratory tests in free space, the operation range of the modified wireless link was up to 5 m. Tests and their results in an environment with real concrete waste containers is reported in chapter 8.5.2.

8.4 Lab tests

8.4.1 Antenna coupler test system

The hardware design of the wireless link through the steel cover of waste drums, reported in chapter 8.3.1, was based on the earlier performance evaluation of the antenna coupler by a test system, reported in this chapter.

The performance of the antenna coupler through a 1.2 mm ferromagnetic steel plate, provided by UJV, was evaluated by a laboratory test set-up at VTT (Figure 3). The ferrite core antenna of the transponder unit was wired by 1000 turns of 0.21 mm enamelled copper wire. The ferrite core antenna of the reader unit was wired by 300 turns of 0.34 mm enamelled copper wire. The powering and data modulation circuits were implemented on a breadboard.

Figure 4 shows the measured DC-to-DC power transfer efficiency through the ferromagnetic steel plate without any gaps between the ferrite cores and the steel plate. The maximum efficiency (over 1 %) was achieved by carrier frequencies around 50 Hz. The measured efficiency is sufficient for powering simple embedded sensors measuring e.g., temperature, moisture, and pressure.

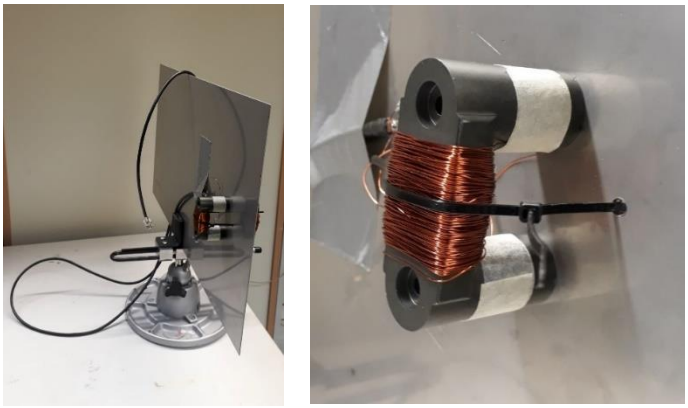

Fig. 3: Antennas of the test system and closer illustration of the reader unit antenna.

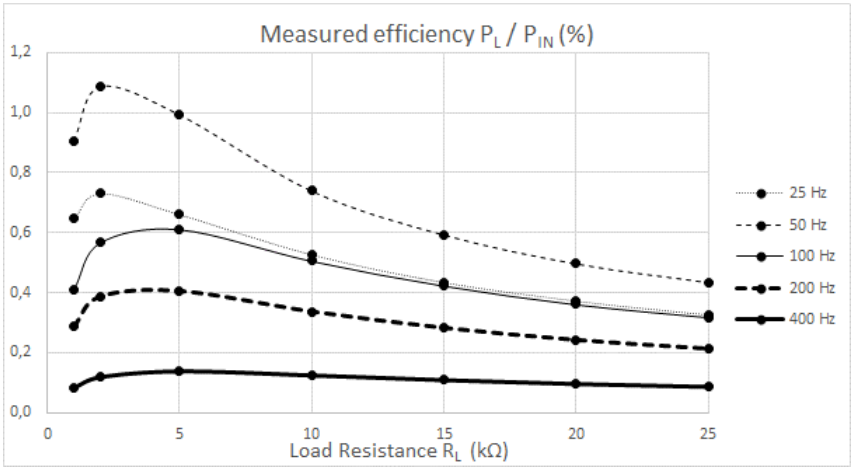

Fig. 4: Measured DC-to-DC power transfer efficiency through the 1.2 mm ferromagnetic steel plate.

Figure 5 shows the data uplink signal graphs through the ferromagnetic steel plate. The data uplink pulses were generated by connecting 3.0 V via a 1 kΩ resistor for 10 ms to the antenna of the transponder unit. The graphs indicate that the signal attenuation by the ferromagnetic steel plate can tolerated, the length of the modulation pulses can be around 1 ms, and the data uplink pulses can be well received and regenerated in the reader unit.
Since the placing of the transponder unit and the reader unit at the opposite sides of the steel cover so that their antennas are exactly focused to each other may be difficult in practice, the effect of the lateral displacement between the antennas was also measured (Figure 6). The degradation of the power transfer efficiency and received modulation pulse amplitude due to a 6 mm lateral displacement were only about 20 % and 10 % respectively, which will not hamper the operation considerably and can be tolerated in practice.
In addition, the effect of a gap between the UR cores and the steel was measured by inserting a 0.5 mm thick acrylic sheet between the steel plate and both antennas (Figure 7). The received data uplink modulation pulses were still clearly detectable (amplitude about 40

% of the original in Figure 5), whereas the degradation of the power transfer efficiency was remarkable. The performance degradation can be partly compensated by modifying the number of turns of the antennas. Still, to maintain a proper power transfer performance, the gap at both sides should be kept below 1 mm, or the total gap below 2 mm.
Another observation from the laboratory test system was that the ferromagnetic steel caused some acoustic noise during the power transfer.

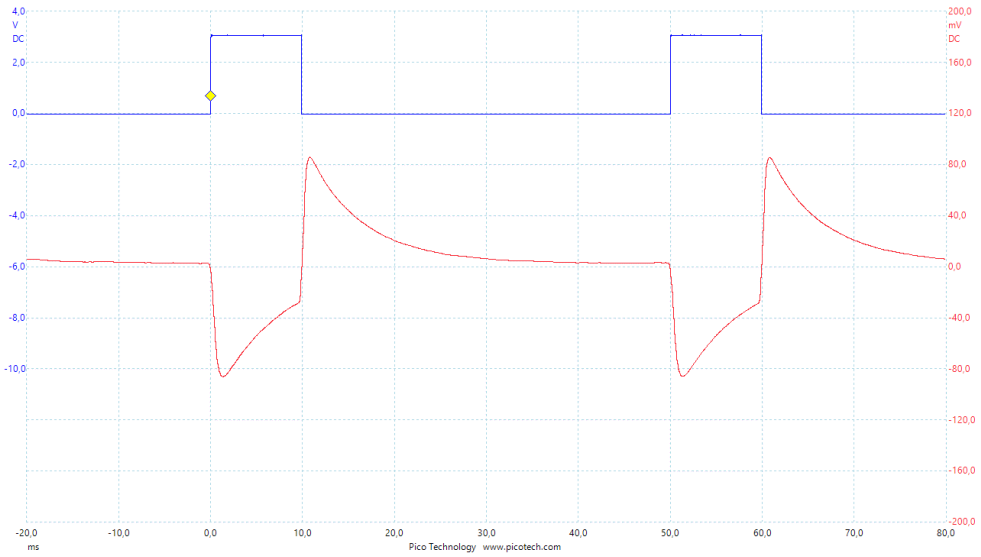

Fig. 5: Measured sensor data uplink pulses. The blue (upper) graph is the original sensor data signal in the transponder unit. The red (lower) graph is the received antenna signal in the reader unit, filtered by 1 kHz low-pass filter.

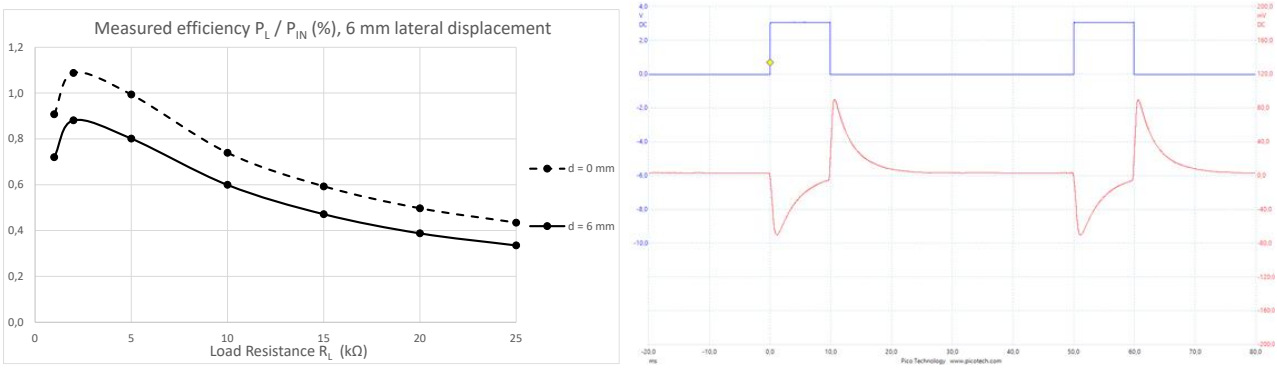

Fig. 6: Measured DC-to-DC power transfer efficiency and received uplink modulation pulses with 6 mm lateral displacement between the antennas. The power transfer efficiency graph without the displacement is included for reference. The carrier frequency was 50 Hz.

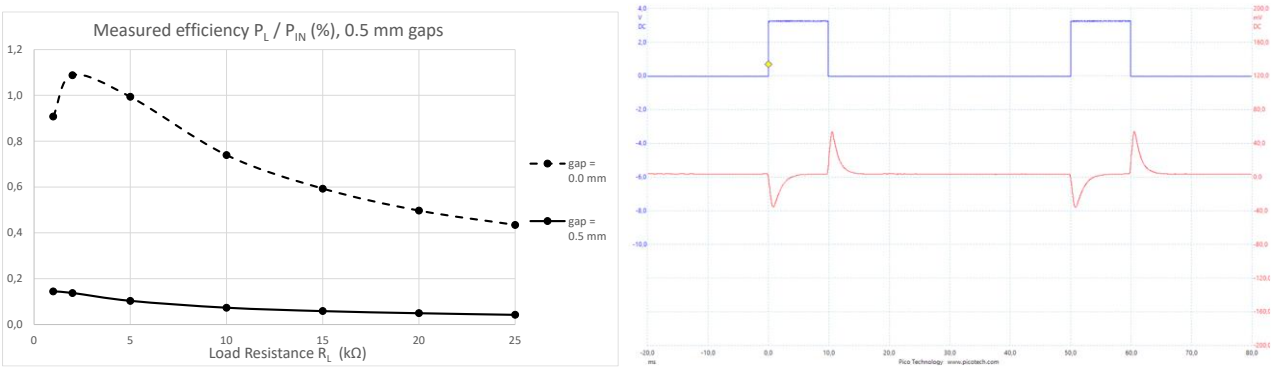

Fig. 7: Measured DC-to-DC power transfer efficiency and received uplink modulation pulses with 0.5 mm gaps between the steel plate and both antennas. The power transfer efficiency graph without the gaps is included for reference. The carrier frequency was 50 Hz.

8.4.2 Wireless link test system

After the evaluation of the performance of the antenna coupler by the test set-up as reported in the previous chapter, printed circuit boards (PCB) and software for the entire wireless link through the steel cover were designed and implemented. Based on them, a more comprehensive test system (Figure 8) was set up. The test system involved a transponder unit with its embedded software, a reader unit, a microcontroller unit with its embedded software, a laptop computer with the GUI software and a Bluetooth dongle, and two SensorNode PCBs provided by BAM.

Fig. 8 Test system of the wireless link through the steel cover of the drum. The components from the left to the right are the transponder unit PCB with a connected antenna and two SensorNode PCBs, the reader unit PCB with a connected antenna, the microcontroller unit with a connection cable to the reader unit, and the laptop computer with GUI software and a Bluetooth dongle (commercial PCB) for the communication with the microcontroller unit.

Figure 9 shows measured signal graphs from the test system through the ferromagnetic steel plate that also illustrate the main activities of the transponder unit and the voltage of its interim energy storage during them with one connected SensorNode. The horizontal axis

is the time in seconds. At 0 s, the interim energy storage voltage (blue graph) reaches 6.3 V, which causes the energy reception circuit to switch on the microcontroller supply voltage (red graph). After initializing itself, the microcontroller software switches on the supply voltage of the SensorNode (yellow graph), reads the sensor data and switches off the SensorNode supply voltage. The energy download from the reader unit (green graph) stops at 0.7 s, after which the microcontroller software waits 2.3 s for the stabilization of the antenna circuit of the reader unit, and sends the data uplink message (green graph) starting at 3.0 s. After finishing this, the microcontroller software starts to discharge residual energy from the interim energy storage, which causes the energy reception circuit to switch off the microcontroller supply voltage when the interim energy storage voltage has sunk below 3.2 V.

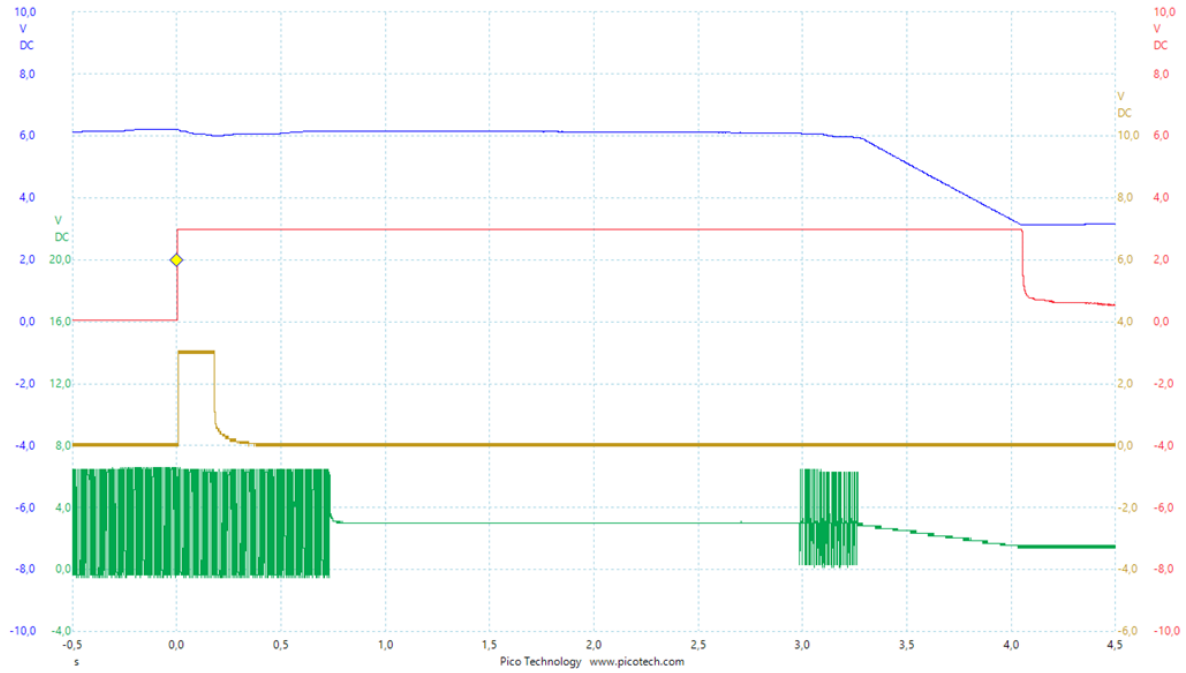

Fig. 9: Measured signals from the transponder unit with one SensorNode. The blue graph is the voltage of the interim energy storage. The red graph is the microcontroller supply voltage. The green graph is the antenna signal showing first the tail end of the energy reception and later the transmission of a sensor data uplink message. The yellow graph is the SensorNode supply voltage.

8.5 Tests in a realistic environment

8.5.1 Wireless link through the steel lid

The transponder unit and the reader were supplemented by 3D-printed plastic encapsulations designed and manufactured by BAM. The thickness of the material between the antenna ferrite cores and the lid was 0.5 mm at both sides of the lid. The transponder unit and the reader unit were attached onto the steel lid of a mock-up waste drum. The total distance between the antennas, comprised of the 1.5 mm lid, the enclosures and the adhesive between the lid and the enclosure, was about 3 mm. Five SensorNodes were connected to the transponder unit. The operation of this set-up was tested at BAM (Figure 10).

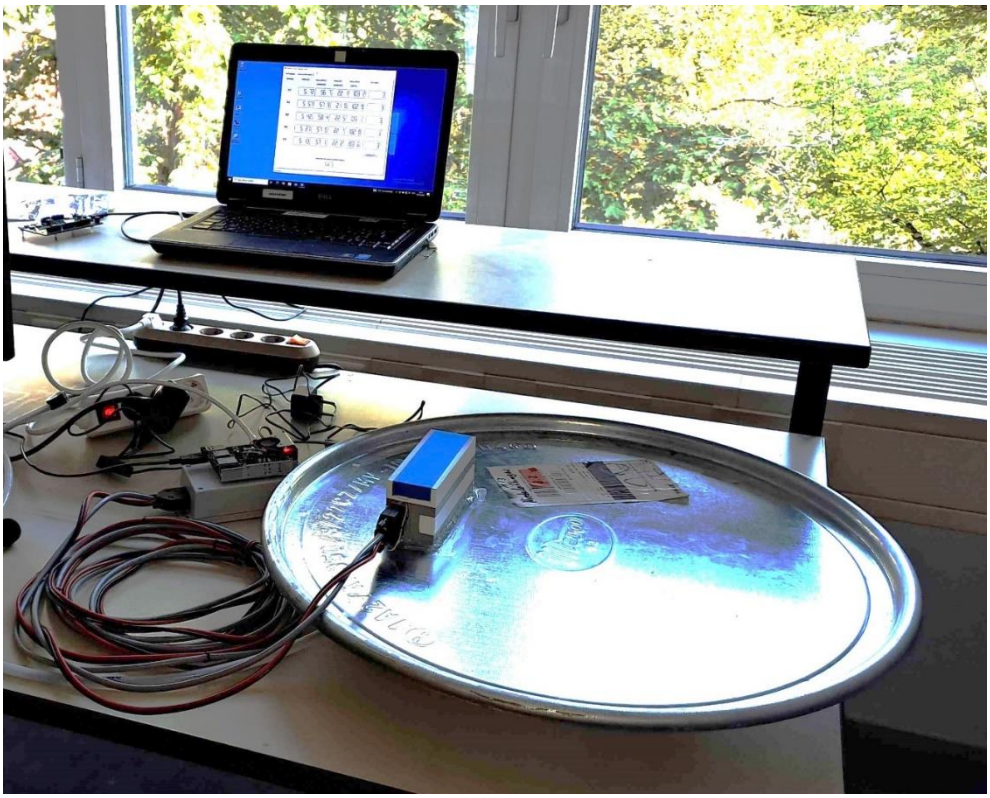

Fig. 10: Testing the wireless link through the steel lid of a mock-up waste drum at BAM. The transponder unit (not visible) is on the bottom side of the lid.

Figure 11 shows measured signal graphs from one data acquisition cycle of the five SensorNodes connected to the transponder unit. The blue, red and green graphs represent the sequence of the five data packets measured, respectively, from the transponder unit, the reader unit, and the microcontroller unit. The received data signal by the microcontroller unit (green) is congruent to the transmitted data signal by the transponder unit (blue) but inverted.

Each data packet represents one SendorNode and consists of 38 data pulses, encoding the drum ID, SensorNode ID, the measured voltage of the interim energy storage, measured sensor readings (humidity, temperature, pressure) by 16-bit integers, and an 8-bit CRC checksum. There are also two dummy pulses before the first SensorNode message, since the first pulse after the energy download is often defectively received, which also can be

seen from the red graph. The expected reason for this is the residual magnetic energy after the energy download due to the magnetic hysteresis of the steel lid.
The interim energy storage in the transponder unit is 1.1 mF electrolytic capacitor that is charged to 6.3 V – 8.0 V during the energy download cycle. This takes about half a minute, during which the power consumption of the reader unit and the microcontroller unit is totally 4.5W. The yellow graph behind the red graph in Figure 11 is the voltage of the interim energy storage that in this configuration drops from 5.75 V to 5.0 V during the five data uplink messages. Thus, sending an uplink data message of one SensorNode takes 150 mV from the interim energy storage.

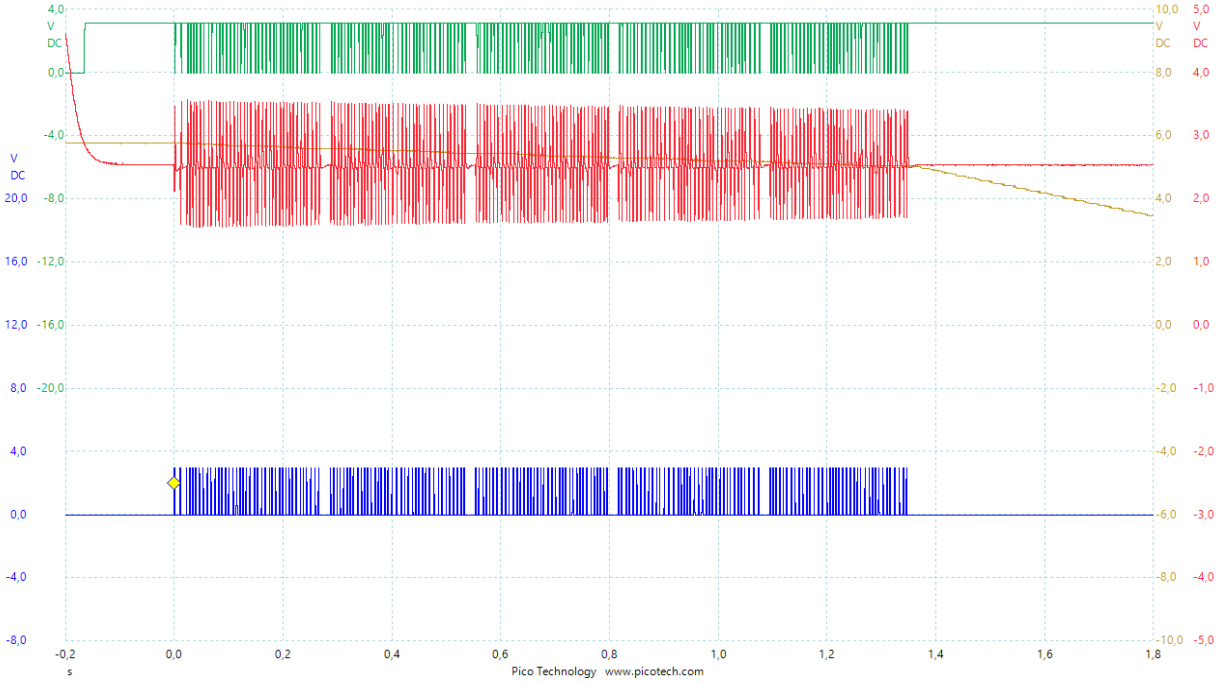

Fig. 11: Measured graphs of the data uplink messages of five connected SensorNodes. The blue graph is the transmitted data from the microcontroller in the transponder unit. The red graph is the received analog data signal in the reader unit, and the green graph is the regenerated data signal in the microcontroller unit. The last one (green) is congruent to the first one (blue) but inverted. The yellow graph behind the red graph is the voltage of the interim energy storage in the transponder unit.

In general, the energy download from the reader unit to the transponder unit and the data uplink in the opposite direction through the steel lid operated as expected. However, sporadic losses of uplink data messages from the transponder unit to the reader unit were observed. The expected reason for this is the timing skew of the received data pulses, caused by magnetic hysteresis of the lid steel.

8.5.2 Wireless link for monitoring concrete containers

The operation of the wireless link test system with modified radio technology according to chapter 8.3.4 was evaluated and demonstrated in January 2024 in the KAJ storage of TVO, Olkiluoto, Finland. The size of the concrete boxes was 2.74 m x 2.74 m x 1 m. Applied test set-ups were:

- Figure 12: The transponder unit antenna was placed on the outer side of a concrete container. The reader unit antenna was placed in front of the concrete container.
- Figure 13: The placement of the transponder unit antenna was as in the previous set-up, but the reader unit was placed to the opposite side of the container (data acquisition through a concrete container).
- Figure 14: The transponder antenna was placed on the inner side of a concrete container filled with waste drums.
- Reference measurements in free space.

Fig. 12: Test set-up with the transponder unit antenna on the outer side of a concrete container. The leftmost photo is the transponder unit and the rightmost photo the antenna of the reader unit at the same side of the container.

© TVO

Fig. 13: Test set-up for data acquisition from the transponder unit through a concrete container.

© TVO

Fig. 14: Test set-up with the transponder unit antenna on the inner side of a concrete container with waste drums.

The test system was able to power and read a SensorNode PCB connected to the transponder unit in all test set-ups. Closer results of the performance measurements are in Table 1.

Table 1: Summary of the wireless performance measurements of each test set-up.

	Wireless distance	transponder antenna Q-factor	Energy transfer efficiency	SensorNode data acquisition
Transponder unit antenna on the outer side (Figure 12)	3.0 m	16.3	240 ppm	OK
Transponder unit antenna on the outer side, data acquisition through the container (Figure 13)	3.4 m	16.3	160 ppm	OK
Transponder unit antenna on the inner side (Figure 14)	2.1 m	12.5	260 ppm	OK
Reference measurements in free space	3.4 m	48.1	1140 ppm	OK

The placement of the transponder unit antenna affected to its inductance and Q-factor. These antenna parameters were measured and the antenna tuning re-adjusted separately for each placement. A notable observation from the energy transfer efficiency measurement results is the small difference between the first and the second test set-up. These results indicate that the main reason for the wireless performance degradation in concrete containers with relation to the free space is the effect of the materials in the immediate vicinity of the antennas. The effect of the materials more far away (>~1m) is smaller. Another notable observation is the shorter wireless operation range in the third test set-up, which is probably due to the damping of the radio signal by the metallic waste drums close to the transponder unit antenna.
A conclusion is that the wireless data acquisition of batteryless low-power sensors in the outermost concrete containers in their storage room is technically feasible with a wireless arrangement according to the test system. It is also possible to access these sensors partly in the inner containers. However, wireless distances over 3 m through the containers would require bigger antennas and/or improving the RF electronics in the transponder and reader units. A fundamental limitation is also that when the wireless range is several times longer that the antenna diameter of the reader unit, the power transfer efficiency even in free space decays to the sixth power of the distance between the antennas. This limits the maximum operation range in practice to around fivefold over the antenna diameter of the reader unit.

8.6 Summary and outlook

A data acquisition system for low-power batteryless sensors inside waste drums by wireless link through the steel cover of the drum has been designed and tested in project PREDIS. The tests have shown the feasibility of powering and data readout of the sensors without any perforations of the steel cover, thus preserving the integrity of the waste drum. From the basic functionality, the developed wireless link is similar to the existing RFID technologies. However, because of the operation through the steel cover of the drum, the technical implementation differs much from the existing RFID technologies.
In the tests through the lid of a waste drum made of 1.5 mm ferromagnetic steel, the developed wireless link operated as expected. Occasionally, sporadic uplink data messages

from the transponder unit to the reader unit were lost. The expected reason for this is the timing skew of the received data pulses caused by magnetic hysteresis of the lid steel. This can be improved by modifying the modulation parameters of the data uplink to tolerate more timing inaccuracy of the received data pulses. The developed wireless link would be able to operate through much thicker layers of non-magnetic steel and many other metals without this problem.
In addition to embedded monitoring of the waste drums, another possible application of the developed technology is wireless monitoring of bigger reinforced concrete containers in their storage spaces. This was successfully tested by a batteryless sensor and the same data acquisition system with modified radio parts.

8.7 References

[1] ISO/IEC 14443-1, in Cards and security devices for personal identification. Contactless proximity objects. Part 1: Physical characteristics. 2018.
[2] ISO/IEC 15693-1, in Cards and security devices for personal identification. Contactless vicinity objects. Part 1: Physical characteristics. 2018.
[3] Yamakawa, M., et al., Wireless Power Transmission into a Space Enclosed by Metal Walls Using Magnetic Resonance Coupling. Wireless Engineering and Technology, 2014. 5: p. 19-24.
[4] Vu, T.A., et al., Wireless power transfer through metal using inductive link. International Journal of Power Electronics and Drive Systems (IJPEDS), 2019. 10: p. 1906.